Volume 4 APRIL, 1933 Number 4

PHYSICS

A Journal of General and Applied Physics

Potential Distribution About an Electrode on the Surface of the Earth

MORRIS MUSKAT, *Gulf Research Laboratory, Pittsburgh, Pennsylvania*

(Received February 20, 1933)

An analytical study is made of the potential distribution about an electrode on a stratified earth, from the point of view of developing special formulas appropriate for computation at small and large distances from the electrode. Power series in the distance for small distances and simple asymptotic expansions for large separations are derived first for a two layer earth, from integral expressions for the potentials. For graphical integration a transformation is derived which makes the integrals converge very rapidly. For a many layer earth a general method for deriving the power series for small distances is indicated. For large distances, general expansions are given in closed (Eq. (23)) and asymptotic forms (Eq. (24)) applying to all types of conductivity variation. Explicit expressions for the power series are given for a three layer earth with the middle layer of thickness equal to and twice that of the upper layer. Closed and very rapidly converging series of Hankel function expansions are then developed for the third layer having zero or infinite conductivities, with the thickness of the middle layer being equal to, twice and three times that of the upper layer. Thirty numerical cases have been computed and plotted as curves to illustrate the fundamental formulae developed. In an appendix general proofs are given for the asymptotic expansions of not only the type of integrals occurring in the present problem but also for integrals involving Weber and Hankel functions as well as the Bessel functions, and where these functions are of non-zero orders.

INTRODUCTION

A GREAT deal of work has been done on the problem of the potential distribution about a point electrode placed on the earth's surface, the earth being supposed to consist of two or more plane faced layers of different conductivities. Thus as long ago as 1873 Maxwell[1] set up the system of images with which to treat the problem. Recently the problem has again attracted attention. Curves for the potential distribution, but without the analysis, were given by Weaver.[2] Following these, formulae in terms of images, but without explicit derivation, were published by Hummel.[3] Stefanesco and Schlumberger[4] then gave a derivation of Hummel's formulae by a direct solution of Laplace's equation in terms of Bessel functions. Finally, Roman[5] published extensive numerical tables for the computation of the potential distribution, for a two layer earth.

Although these investigations have provided a number of numerical solutions nothing seems to have been given in the sense of a detailed analytical discussion of the formal solutions. In connection with the problem of the flow of underground waters in artesian wells,[6] the writer had occasion to study in detail the potential distribution about an electrode in an insulated place faced conducting slab. Because of the great geophysical interest in the more general problem of several conducting slabs it was thought worthwhile to generalize the methods of the previous analysis and apply them to the case of several conducting slabs. In the present paper we shall first present the generalizations applying

[1] J. C. Maxwell, *Electricity and Magnetism*, 1873.

[2] W. Weaver, Amer. Inst. Min. and Met. Eng. Tech. Pub. 121, 1928.

[3] J. N. Hummel, Zeits. Geophysik **5**, 89, 228 (1929).

[4] S. Stefanesco and C. and M. Schlumberger; J. de Phys. et Rad. **1**, 132 (1930); cf. also L. J. Peters and J. Bardeen; Physics **2**, 103 (1932).

[5] I. Roman; U. S. Bur. Mines, Tech. Paper 502, 1931.

[6] M. Muskat, Physics **2**, 329, 1932.

to the simpler problem of a plane faced surface layer overlying a semi-infinite bed of conductivity different from that of the surface layer and then extend them to the case of a three layer earth. The essential results will be the expressions of the potential distributions near the electrode as power series in the radial distance from the vertical axis through the electrode and as asymptotic expansions in the reciprocal of this distance for large distances from the electrode axis.

I. An Electrode in a Two Layer Earth

We shall base our fundamental formulae upon the solution of Laplace's equation in terms of Bessel functions. Our coordinate system will be chosen as indicated in Fig. 1. The problem then will be to find solutions Φ_1 and Φ_2 of

$$\left.\begin{aligned} &\nabla^2\Phi=0 \\ \text{such that}\quad &\Phi_1=\Phi_2 : z=a/2; \\ &\frac{\partial\Phi_1}{\partial z}=0 : z=0;\ \sigma_1\frac{\partial\Phi_1}{\partial z}=\sigma_2\frac{\partial\Phi_2}{\partial z} : z=\frac{a}{2} \end{aligned}\right\} \tag{1}$$

and so that Φ_1 have a simple pole at $(0, f)$. Before proceeding with the solutions it is convenient to take the unit of length equal to twice the thickness of the surface layer, and introduce the dimensionless variables:

$$w=z/a;\quad \rho=r/a;\quad x=f/a. \tag{1a}$$

With regard to the conductivity constants σ_1, σ_2 it will be useful to introduce both the symbol k, where:

$$k=(\sigma_1-\sigma_2)/(\sigma_1+\sigma_2) \tag{1b}$$

and the quantities γ defined by:

$$\gamma=\operatorname{ctnh}^{-1}(\sigma_2/\sigma_1) : \sigma_2/\sigma_1>1 :$$
$$\gamma=\tanh^{-1}(\sigma_2/\sigma_1) : \sigma_2/\sigma_1<1 \tag{1c}$$

so that:

$$k=-e^{-2\gamma} : \sigma_2/\sigma_1>1 : k=e^{-2\gamma} : \sigma_2/\sigma_1<1. \tag{1d}$$

Although the final results suitable for numerical discussion may be most conveniently expressed in terms of k, the derivation of the formulae of interest may be more directly developed by the use of the symbol γ, and will therefore be employed in most of the formal steps of the analysis, even though this will necessitate the separate treatment of the cases $\sigma_2/\sigma_1>1$ and $\sigma_2/\sigma_1<1$.

Since Stefanesco and Schlumberger[4] have already given the method of solving Eq. (1) by means of Bessel functions we shall state the results only. They are:

$$\left.\begin{aligned} \sigma_1/\sigma_2<1 : w\leq x\leq\tfrac{1}{2} : \Phi_1&=2\int_0^\infty \frac{J_0(2\rho\alpha)\cosh 2\alpha w\sinh(\alpha+\gamma-2\alpha x)d\alpha}{\cosh(\alpha+\gamma)}, \\ \tfrac{1}{2}\geq w\geq x : \Phi_1&=2\int_0^\infty \frac{J_0(2\rho\alpha)\cosh 2\alpha x\sinh(\alpha+\gamma-2\alpha w)d\alpha}{\cosh(\alpha+\gamma)}, \\ w\geq\tfrac{1}{2}\geq x : \Phi_2&=2\sinh\gamma\int_0^\infty \frac{J_0(2\rho\alpha)\cosh 2\alpha x e^{-(2w-1)\alpha}d\alpha}{\cosh(\alpha+\gamma)}, \end{aligned}\right\} \tag{2}$$

$$\left.\begin{aligned} \sigma_1/\sigma_2>1 : w\leq x\leq\tfrac{1}{2} : \Phi_1&=2\int_0^\infty \frac{J_0(2\rho\alpha)\cosh 2\alpha w\cosh(\alpha+\gamma-2\alpha x)d\alpha}{\sinh(\alpha+\gamma)}, \\ \tfrac{1}{2}\geq w\geq x : \Phi_1&=2\int_0^\infty \frac{J_0(2\rho\alpha)\cosh 2\alpha x\cosh(\alpha+\gamma-2\alpha w)d\alpha}{\sinh(\alpha+\gamma)}, \\ w\geq\tfrac{1}{2}\geq x : \Phi_2&=2\cosh\gamma\int_0^\infty \frac{J_0(2\rho\alpha)\cosh 2\alpha x e^{-(2w-1)\alpha}d\alpha}{\sinh(\alpha+\gamma)}. \end{aligned}\right\} \tag{3}$$

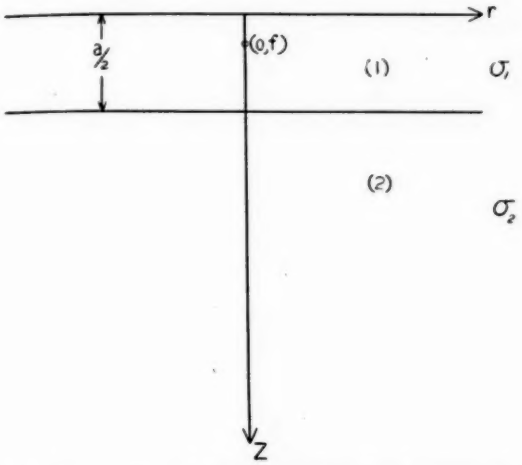

FIG. 1. Diagrammatic representation of an electrode, at $(0, f)$ in a two layer earth.

Eqs. (2) and (3) are essentially equivalent to those of Stefanesco and Schlumberger, being only somewhat more symmetrical than the corresponding formulae already in the literature. The symmetry has been attained by the introduction of the quantity γ rather than the k of Eq. (1b). On the other hand, the analysis of Stefanesco and Schlumberger really went no further than the demonstration that their equivalents of Eqs. (2) and (3) could be evaluated in the form of the series of images already given by Hummel. Here, however, we shall begin with these equations and derive from them separate expansions suitable for numerical treatment when ρ is small and when ρ is large.

A. Expansions for small values of ρ

To study these solutions for small value of ρ we shall expand the denominators in Eqs. (2) and (3) as:

$$\left.\begin{aligned}\operatorname{sech}(\alpha+\gamma) &= 2\sum_0^\infty n(-1)^n e^{-(2n+1)(\alpha+\gamma)} \\ \operatorname{csch}(\alpha+\gamma) &= 2\sum_0^\infty n e^{-(2n+1)(\alpha+\gamma)}\end{aligned}\right\}. \quad (4)$$

We might now integrate term by term on using the relation:

$$\int_0^\infty e^{-ay} J_0(by)\,dy = (a^2+b^2)^{-\frac{1}{2}}, \quad (4a)$$

obtaining at once Hummel's series of images with terms of the form

$$e^{-2n\gamma}/[\rho^2+(n\pm w\pm x)^2]^{\frac{1}{2}}.$$

These could then be individually expanded as power series in ρ and summed. It will be more convenient, however, to expand $J_0(2\rho\alpha)$ and then integrate the double series. For purposes of brevity we shall restrict ourselves to the problem of most practical interest—the potential distribution on the earth's surface due to an electrode on the surface, i.e., the case where $w=x=0$. Furthermore, since we shall consider only the function Φ_1, we shall drop the subscript. Carrying out, then, the procedure indicated, and returning to the notation of Eq. (1b) we find:

$$\Phi = 1/\rho + 2\sum_0^\infty m(-1)^m[(1\cdot 3\cdots 2m-1)/(2\cdot 4\cdots 2m)]\rho^{2m}\sum_1^\infty n\,k^n/n^{2m+1}. \quad (5)$$

If $k=0$, i.e., if there is no conductivity contrast between the two media, then $\Phi=1/\rho$, as it should be for the surface potential due to an electrode embedded in the surface of a semi-infinite *homogeneous* medium. If, however, the conductivity contrast is nonvanishing, $|k|>0$, the series have to be summed.

In doing this it is convenient to take out and sum separately the terms for $m=0$ (the constant terms) and those for $n=1$ and 2, corresponding to the images nearest the electrode. Eq. (5) can then be rewritten as:

$$\Phi = 1/\rho - 2\log(1-k) - 2k - k^2 + 2k/(1+\rho^2)^{\frac{1}{2}} + 2k^2/(4+\rho^2)^{\frac{1}{2}} + 2\sum_1^\infty m(-1)^m c_m f_m(k)\rho^{2m}, \quad (6)^7$$

[7] The constants independent of ρ have to be retained in order to make the above Φ connect with that to be derived later for large ρ from the same integrals of Eq. (2) and Eq. (3).

where

$$c_m=(1\cdot 3\cdots 2m-1)/(2\cdot 4\cdots 2m);\quad f_m(k)=\sum_3^\infty n\,k^n/n^{2m+1}. \tag{7}$$

The series for $f_m(k)$ evidently converges very rapidly even if $k\sim 1$. Its value, in fact, will always be of the order of $k^3/3^{2m+1}$. Hence, since $c_m=0(1/m)^{\frac{1}{2}}$ for m large, the radius of convergence of the series in Eq. (7) is given by $|\rho|=3$.[8] Thus, whereas the direct image series converges essentially as k^n/n, the expansion of Eq. (6) converges in ρ as $\rho^{2m}/3^{2m}$.

It is of interest to note that if only the terms for $m=0$ are separated from Eq. (5) it will reduce, for the case $\sigma_2=0$, $(k=1)$ to:

$$\Phi=1/\rho-2\log(1-k)+2\sum_1^\infty m(-1)^m c_m\zeta(2m+1)\rho^{2m}$$

where ζ is the zeta-function. This is equivalent to Eq. (7) in the analysis of the problem of the insulated conducting slab previously treated by the author,[6] as of course it should for $\sigma_2=0$.

Before illustrating the use of Eq. (6) numerically, we shall develop the corresponding expressions suitable for large values of ρ.

B. Asymptotic expansions for Φ for large ρ

To study our potential function for large values of ρ it is convenient to return again to the integral expressions of Eqs. (2) and (3). However, we cannot simply expand sech $(\alpha+\gamma)$ and csch $(\alpha+\gamma)$ as in Eq. (4) and then apply the asymptotic expansion for $J_0(2\rho\alpha)$. For as the asymptotic expansion of $J_0(2\rho\alpha)$ involves terms as $1/(\alpha)^n$ with $n>1$ the resulting integrals would diverge at $\alpha=0$. Neither could we expand directly the image series of terms like $e^{-2n\gamma}/(\rho^2+n^2)^{\frac{1}{2}}$, since even if ρ is large, there will always be terms for which $n>\rho$.

Before, however, proceeding with the derivation of a real asymptotic expansion for Φ it may be of interest to note that if one wishes to integrate Eqs. (2) and (3) graphically a more suitable form, especially for large ρ, may be obtained as follows. First, J_0 may be split into the two Hankel integrals as:

$$2J_0(2\rho\alpha)=H_0^{(1)}(2\rho\alpha)+H_0^{(2)}(2\rho\alpha).[9]$$

The two separate integrals formed in this way (from the original integrals of Eqs. (2) or (3)) may then be taken with contours in the complex α plane; the integral with $H_0^{(1)}(2\rho\alpha)$ may be carried over the infinite first quadrant arc and down the + imaginary axis, and the integral with $H_0^{(2)}(2\rho\alpha)$ may be carried over the infinite 4th quadrant arc and up the − imaginary axis. Noting then that since $\gamma>0$ there are no poles in these contours, and using the relation:

$$H_0^{(1)}(iz)=-H_0^{(2)}(-iz)=(-2i/\pi)K_0(z),$$

Eqs. (2) and (3), in the notation of Eq. (1b) reduce to:

$$\left.\begin{aligned} w\leq\tfrac{1}{2}:\Phi_1&=\frac{2}{\pi}(1-k^2)\int_0^\infty\frac{K_0(\rho\mu)\cos w\mu\cos x\mu\,d\mu}{1+k^2-2k\cos\mu},\\ w\geq\tfrac{1}{2}:\Phi_2&=\frac{2}{\pi}(1+k)\int_0^\infty\frac{K_0(\rho\mu)\cos x\mu(\cos\mu w-k\cos\mu(1-w))d\mu}{1+k^2-2k\cos\mu}.\end{aligned}\right\} \tag{8}$$

Since K_0 vanishes exponentially for large arguments Eq. (8) is convenient for graphical integration for large ρ, unless $k\sim+1(\sigma_2\sim 0)$. The case $k\sim-1$, however, will cause but little

[8] This radius of convergence could be advanced by separating out still further image terms, as those corresponding to $n=3$, and $n=4$. On the other hand, without any separation, the series of Eq. (5) has a radius of convergence of $|\rho|=1$. It may be noted, too, that Roman's[5] rather lengthy and complex analysis is really equivalent to separating out the terms for $n=1\cdots 5$ and expressing the remainder as a series in $(\rho/10)^2$ with numerical coefficients.

[9] This, and the other relations involving the Bessel or related functions which will be used below, may be found in *Theory of Bessel Functions* by Watson.

difficulty since the minimum of the denominators will occur first at $\mu=\pi$ and even if $\rho=1$, $K_0(\rho\mu)/(1+k)^2<3$ for k as small as -0.90.

On the other hand, Eq. (8) is unsuited for the derivation of an asymptotic expansion. For if $K_0(\rho\mu)$ be expanded under the integral sign the same difficulties will arise as in the case of the expansion of J_0 in the original Eqs. (2) and (3). We have therefore to resort to quite a different method; and since we shall be able to express Φ_1 in a rigorous closed series form (cf. Eqs. (11) (12) below) we shall treat the more general case where w, $x\neq 0$, but carry through the details only for $\sigma_1/\sigma_2<1$ and drop the subscripts. Thus by the "partial fraction" rule we have:

$$\left.\begin{aligned}\frac{\cosh 2\alpha w \sinh(\alpha+\gamma-2\alpha x)}{\cosh(\alpha+\gamma)} &= \sum_{\substack{\text{odd}\\>0}} n\, 1/((\alpha+\gamma)^2+n^2\pi^2/4)\\ \cdot[(\alpha+\gamma)\{\cosh 2\gamma(w+x)\cos n\pi(w+x)+\cosh 2\gamma(w-x)\cos n\pi(w-x)\}&\\ +n\pi/2\{\sinh 2\gamma(w+x)\sin n\pi(w+x)+\sinh 2\gamma(w-x)\sin n\pi(w-x)\}].&\end{aligned}\right\} \tag{9}$$

We now apply the relations:

$$(\alpha+\gamma)/((\alpha+\gamma)^2+n^2\pi^2/4)=\int_0^\infty e^{-(\alpha+\gamma)y}\cos n\pi y/2dy,$$

$$n\pi/2/((\alpha+\gamma)^2+n^2\pi^2/4)=\int_0^\infty e^{-(\alpha+\gamma)y}\sin n\pi y/2dy,$$

and then integrate Eq. (2) with respect to α, making use of Eq. (4a), finding:

$$\left.\begin{aligned}\Phi=2\sum_{\substack{\text{odd}\\>0}} n\Big[&\{\cosh 2\gamma(w+x)\cos\pi n(w+x)+\cosh 2\gamma(w-x)\cos\pi n(w-x)\}\int_0^\infty \frac{e^{-2\gamma\rho y}\cos\pi n\rho y}{(1+y^2)^{\frac{1}{2}}}dy\\ &+\{\sinh 2\gamma(w+x)\sin\pi n(w+x)+\sinh 2\gamma(w-x)\sin\pi n(w-x)\}\int_0^\infty \frac{e^{-2\gamma\rho y}\sin\pi n\rho y}{(1+y^2)^{\frac{1}{2}}}dy\Big].\end{aligned}\right\} \tag{10}$$

We now observe that:

$$\int_0^\infty e^{-ky}dy/(1+y^2)^{\frac{1}{2}}=(\pi/2)(\overline{H}_0(k)-Y_0(k)), \tag{10a}$$

where $\overline{H}_0$ denotes the Struve function of zero order and Y_0 is the Weber function, in Watson's notation. We, therefore, have finally:

$$\sigma_1/\sigma_2<1;\quad k<0;\quad \tfrac{1}{2}\geq w;$$

$$\left.\begin{aligned}\Phi=\pi\sum_{-\infty}^{+\infty} n\{&\cosh w(2\gamma-(2n+1)\pi i)\cosh x(2\gamma-(2n+1)\pi i)\}\\ &\cdot\{\overline{H}_0(2\gamma\rho-(2n+1)\pi i\rho)-Y_0(2\gamma\rho-(2n+1)\pi i\rho)\}\end{aligned}\right\} \tag{11}$$

and similarly for $\sigma_1/\sigma_2>1$: $k>0$; $\frac{1}{2}\geq w$;

$$\Phi=\pi\sum_{-\infty}^{+\infty} n\{\cosh 2w(\gamma-n\pi i)\cosh 2x(\gamma-n\pi i)\}\cdot\{\overline{H}_0(2\gamma\rho-2n\pi i\rho)-Y_0(2\gamma\rho-2n\pi i\rho)\}. \tag{12}$$

Although these equations really contain the final result of our analysis for this section we shall restrict our further discussion to the special case of most practical interest: $w=x=0$. We have then,

$$\sigma_1/\sigma_2<1 : k<0 : w=x=0$$

$$\Phi=2\int_0^\infty J_0(2\rho\alpha)\tanh(\gamma+\alpha)d\alpha=\pi\sum_{-\infty}^{+\infty}n\{\overline{H}_0(2\gamma\rho-(2n+1)\pi i\rho)-Y_0(2\gamma\rho-(2n+1)\pi i\rho)\}. \quad (11a)$$

$$\sigma_1/\sigma_2>1 : k>0; \quad w=x=0;$$

$$\Phi=2\int_0^\infty J_0(2\rho\alpha)\operatorname{ctnh}(\gamma+\alpha)d\alpha=\pi\sum_{-\infty}^{+\infty}n\{\overline{H}_0(2\gamma\rho-2n\pi i\rho)-Y_0(2\gamma\rho-2n\pi i\rho)\}. \quad (12a)$$

Making use now of the asymptotic expansion of the Struve function $\overline{H}_0$, which is given by

$$\overline{H}_0(z)=Y_0(z)+\frac{1}{\pi^2}\sum_{m=0}^{p-1}(-1)^m\frac{\Gamma^2(m+\frac{1}{2})}{(\frac{1}{2}z)^{2m+1}}+0(z^{-2p-1}) \quad (13)$$

and then, summing the series with respect to n, we get finally:

$$\sigma_1/\sigma_2<1 : k<0; \quad w=x=0;$$

$$\Phi=-\frac{1}{\pi}\sum_0^{p-1}m\frac{(-1)^m\Gamma^2(m+\frac{1}{2})}{\Gamma(2m+1)\rho^{2m+1}}\frac{\partial^{2m}}{\partial\gamma^{2m}}\tanh\gamma+0(\rho^{-2p-1}); \quad (14)$$

$$\sigma_1\sigma_2>1 : k>0; \quad w=x=0;$$

$$\Phi=-\frac{1}{\pi}\sum_0^{p-1}m\frac{(-1)^m\Gamma^2(m+\frac{1}{2})}{\Gamma(2m+1)\rho^{2m+1}}\frac{\partial^{2m}}{\partial\gamma^{2m}}\operatorname{ctnh}\gamma+0(\rho^{-2p-1}). \quad (15)$$

Since $\tanh\gamma$ and its derivatives are always less than 1 except for the numerical factors developing on successive differentiations, and as $\Gamma^2(m+\frac{1}{2})/\Gamma(2m+1)\sim 1/2^{2m}(m)^{\frac{1}{2}}$ for large m, the series of Eq. (14) will be quite suitable for numerical purposes even though in a strict sense it is a divergent series. Eq. (15), on the other hand, is not satisfactory when γ is small ($k\sim 1$, $\sigma_1/\sigma_2>>1$) unless ρ is so large that even $\gamma\rho$ is large. For moderate values of ρ and small values of γ we may derive a more satisfactory series by separating out in Eq. (12a) the term with $n=0$. Carrying through the rest of the analysis as before we get:

$$w=x=0 : \sigma_1/\sigma_2>1;$$

$$\Phi=\pi\{\overline{H}_0(2\gamma\rho)-Y_0(2\gamma\rho)\}+\frac{1}{\pi}\sum_0^{p-1}m\frac{(-1)^m\Gamma^2(m+\frac{1}{2})}{\rho^{2m+1}\Gamma(2m+1)}\left(\frac{\partial^{2m}}{\partial\gamma^{2m}}\operatorname{ctnh}\gamma-\frac{\Gamma(2m+1)}{\gamma^{2m+1}}\right), \quad (15a)$$

where the values of $\overline{H}_0$ and Y_0 may be taken from the tables of Watson.

Although Eqs. (14) and (15) are rather compact analytically their physical significance may be somewhat clearer if expressed explicitly in terms of the conductivity ratios σ_1/σ_2. Carrying out the differentiations for the first four terms we find that both for $\sigma_1/\sigma_2>1$ and $\sigma_1/\sigma_2<1$ the potential for $x=w=0$ has the form:

$$\Phi=\frac{\sigma_1}{\sigma_2\rho}\left[1+\frac{1}{4\rho^2}\left(1-\frac{\sigma_1^2}{\sigma_2^2}\right)-\frac{3}{16\rho^4}\left(1-\frac{\sigma_1^2}{\sigma_2^2}\right)\left(\frac{3\sigma_1^2}{\sigma_2^2}-2\right)+\frac{5}{64\rho^6}\left(1-\frac{\sigma_1^2}{\sigma_2^2}\right)\left(17-60\frac{\sigma_1^2}{\sigma_2^2}+45\sigma_1^4/\sigma_2^4\right)\right]. \quad (16)$$

Before entering now upon a numerical discussion of Eqs. (14) and (15) we must point out that they are not to be used in the limiting cases where $\gamma=0$. Thus, in the case of Eq. (14) where $\gamma=0$ means that $\sigma_1/\sigma_2=0$ we find at once the fallacious result that Φ vanishes as γ approaches zero.

The difficulty, however, is only apparent. For it is to be remembered that Eqs. (14) and (15) are only *asymptotic expansions* and the fact that $\Phi(\gamma=0)=0$ simply means that when $\gamma=0$ the asymptotic expansion for Φ has a leading term *less than* $1/\rho^n$.[10] And in fact this appears automatically when we put $\gamma=0$ in the rigorously valid Eq. (11a), *before* we develop the asymptotic expansion, for we have then:

$$\Phi(\sigma_1/\sigma_2=\gamma=0)=\pi\sum_{-\infty}^{+\infty}n\{\overline{H}_0((2n+1)\pi i\rho)-Y_0((2n+1)\pi i\rho)\}. \tag{11b}$$

For imaginary arguments we may apply the relation:

$$\overline{H}_0(iz)+\overline{H}_0(-iz)-Y_0(iz)-Y_0(-iz)=(4/\pi)K_0(z), \tag{17}$$

where K_0 is the ordinary Hankel function, so that Eq. (11b) becomes:

$$\Phi(\sigma_1/\sigma_2=\gamma=0)=4\sum_{\text{odd}}n\,K_0(n\pi\rho); \tag{11c}$$

as the Hankel functions vanish exponentially for large arguments we see that $\Phi(\gamma=0)$ has indeed an *exponential* leading term, which from the point of view of an asymptotic expansion is vanishingly small compared to a term as $1/\rho^n$.

In the case of Eq. (15) the situation is just reversed. There, when $\gamma\sim0$, which means that the lower medium is a perfect insulator ($\sigma_2=0$), Φ becomes infinite.

This difficulty, on the other hand, is real from an analytical point of view, as it is known that the potential due to the infinite series of images for this special case diverges. The problem then is to separate out the diverging term as an infinite constant and then use the finite variable part which does have physical significance.[11] This may be readily done by returning to Eq. (12a) which shows that when $\gamma\sim0$ the term with $n=0$ becomes infinite. Separating out this term, applying Eq. (17) and noting that $\overline{H}_0(0)=0$, we find:

$$\Phi(\gamma=0=\sigma_2)=-2\log 2\gamma-1.1544$$
$$+2\log 2/\rho+4\sum_{1}^{\infty}n\,K_0(2n\pi\rho). \tag{18}$$

Thus, the first term on the right contains the diverging element of Φ (and in a manner equivalent to that in Eq. (6)) and the remainder gives the variable part of physical interest. And in fact, this variable part is actually identical with that given previously by the author (cf. reference 6, Eq. (10)) for the special case of an insulated slab. It may be noted, too, that only in this case—where the upper layer is insulated—does the potential at large distances from the electrode vary logarithmically with the distance. For finite conductivities of the lower layer and large ρ, the leading term in Φ is proportional to $1/\rho$. The numerical rate of decrease of Φ with ρ, however, increases continuously from the logarithmic rate for $\sigma_2=0$ to that of $1/\rho$ for $\sigma_2=\sigma_1$ and finally to an exponential decrease for $\sigma_2\sim\infty$. Hence, as will be seen below (cf. Fig. 3) $\Phi\rho$ increases with ρ for $\sigma_2/\sigma_1<1$ but decreases with ρ when $\sigma_2/\sigma_1>1$.

C. Numerical discussion

Since a number of numerical cases for the problem of this section are already to be found in the literature we shall confine our numerical discussion to several illustrations of the formulae we have derived by our analysis. For these we have chosen the cases where the conductivity ratios have the values:

$$\sigma_2/\sigma_1=0.01,\ 0.20,\ 1.0,\ 5.0,\ \infty.$$

Now it will be recalled from Eqs. (6) and (7) that for small values of $\rho(\rho<3)$ our series expansions involve the constants c_m and the functions $f_m(k)$. Since the c_m are independent of k they need be computed only once and they will apply to all values of k. The first 10 values are:

[10] As will be seen later, this point will arise also in the general case of a many layered earth.

[11] This question arises also in our series expansion when ρ is small, for when $k\sim1$ the term $-2\log(1-k)$ in Eq. (6) becomes infinite.

m:	1	2	3	4	5	6	7	8	9	10
c_m:	0.5000	0.3750	0.3125	0.2734	0.2461	0.2256	0.2095	0.1964	0.1855	0.1762

As to the functions $f_m(k)$ the computations are almost as simple. For it is evident from their definition that the series for $f_m(k)$ will converge quite rapidly and in the most unfavorable case where $k=+1$ the values may be deduced from known series. In Fig. 2 we have plotted the first four values of $f_m(k)$ for the range $-1\leq k\leq +1$, which includes all positive values of the ratio σ_2/σ_1. Because of the very rapid fall in the value of f_m with increasing m they have been multiplied by successively increasing factors so that they could be plotted on the same scale. The very fact that this has been necessary shows perhaps most clearly the rapid convergence of the series in Eq. (6).

For large values of $\rho(\rho>3)$, the chosen values of σ_2/σ_1 serve to illustrate the various asymptotic expansions that have been developed for this purpose. Thus, for $\sigma_2/\sigma_1=0.01$, Eq. (12a) was used with the term $n=0$ computed separately from the tables of Watson, and with the terms for $n>0$ developed as a Taylor series in γ, after which Eq. (17) was applied to the first terms of this expansion.[12] For $\sigma_2/\sigma_1=0.20$, Eq. (15a) was found very satisfactory. $\sigma_2/\sigma_1=1.0$ corresponds, of course, to a homogeneous earth and hence gives $\Phi=1/\rho$ everywhere, as also follows from Eq. (16). The case $\sigma_2/\sigma_1=5.0$ was readily computed by Eq. (16), and that for $\sigma_2/\sigma_1=\infty$ was treated by the very rapidly converging series of Eq. (11c).

The results of these calculations are plotted in Fig. 3. To avoid the overlapping of the curves and the consequent masking of the effects of the variation of σ_2/σ_1, the function $\Phi\rho$ has been plotted rather than Φ itself. Since curves of this type are already available in the literature we shall not discuss them further. However, we do wish to point out the practical value of the formulae developed here with respect to the

[12] The result of these steps was to give, first, Eq. (18) and then a small correction term proportional to γ.

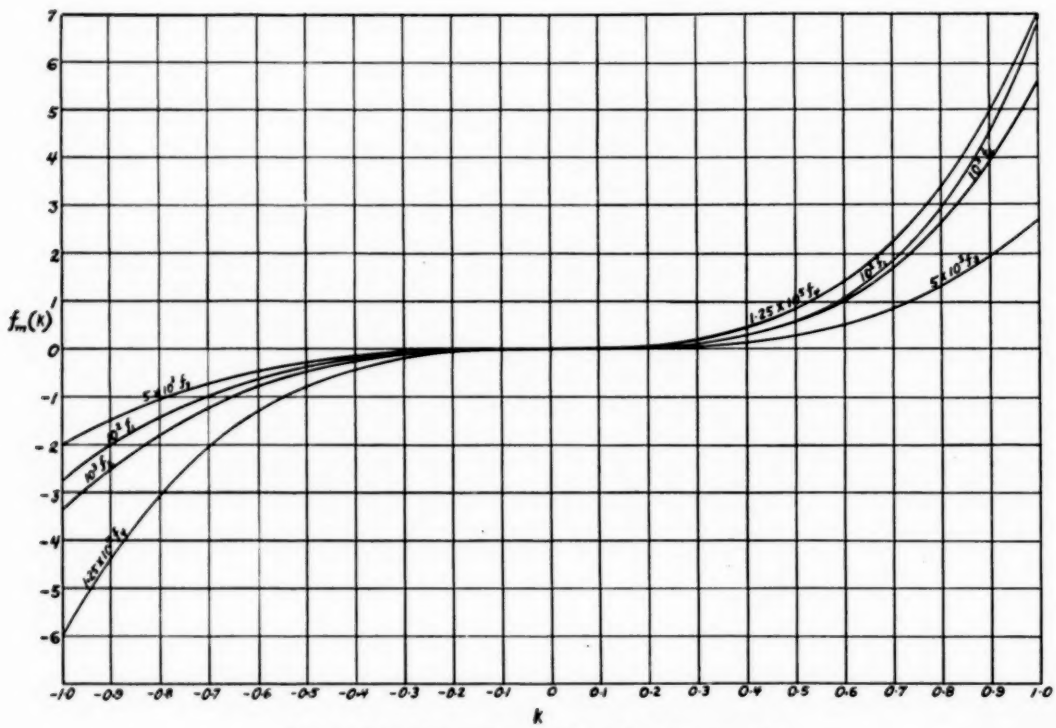

FIG. 2. Plot of functions $f_m(k)$, defined by Eq. (7).

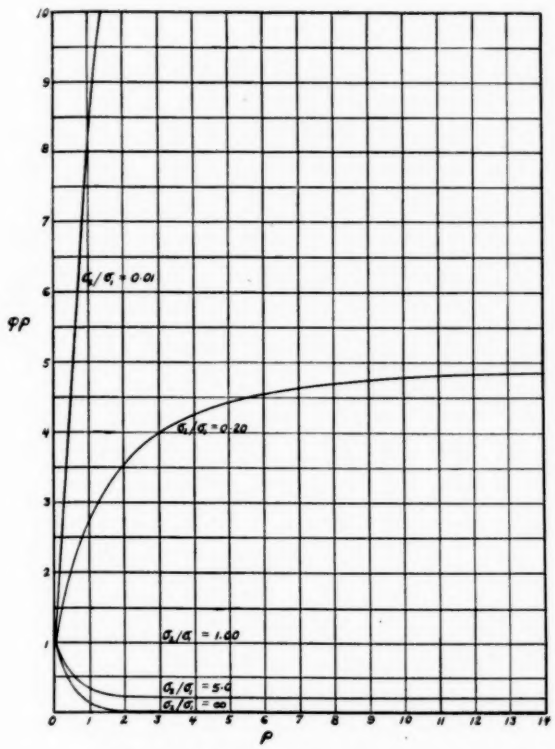

FIG. 3. Surface potential distribution in a two layer earth σ_1 = conductivity of surface layer, σ_2 = conductivity of lower layer. ρ = (radial distance from electrode)/(twice the thickness of upper layer).

calculation of such curves. For in the computations by Eq. (6) one may drop the series after the first four terms and introduce an error of less than 0.6 percent in $\Phi\rho$ even with $\rho=2.0$ and $|k|\sim 1$, for $\sigma_2/\sigma_1<1$. For $\sigma_2/\sigma_1>1$ the errors are somewhat larger, but if necessary a few more terms may be used, each additional term reducing the error at least by the factor 4/9. On the other hand, as the potential distributions must be used graphically for practical applications very high accuracy will seldom be required. Finally, it may be noted that the series of Eq. (6) is an alternating series and hence permits a direct estimate of the errors introduced on terminating it at any given term.

With regard to the large values of ρ, the situation is still more favorable. For in the limiting cases $\sigma_2/\sigma_1=\infty$ and $\sigma_2/\sigma_1=0.01$ the use of the Hankel functions gives high accuracies with only two or three terms of the series. In the intermediate cases for $\sigma_2/\sigma_1<1$ the series of Eq. (15a) for the smaller values of $\rho(\rho\sim 2)$ begin to diverge after the first two terms and must necessarily be dropped thereafter; since it may be proved that the remainders of the asymptotic expansions developed here are smaller in absolute value than the last term retained, the accuracy is not impaired (for $\sigma_2/\sigma_1=0.20$, $\rho=2$, the remainder after the first two terms was 0.1 percent). When $\sigma_2/\sigma_1>1$ the series do not diverge so rapidly and even though $\Phi\rho<1$, three terms in Eq. (16) will in most cases already leave errors less than $\frac{1}{2}$ percent.

These results compare favorably with the laborious calculations required when the series of images are summed directly. For the convergence of these series, except when $k\sim 0$, is so slow that to obtain accurate results as many as 100 terms may at times be necessary.[13]

II. Potential Distribution in a Stratified Earth with More Than Two Layers

A. General theory

When there are more than two layers to be considered the numerical discussion immediately becomes much more complicated. The formal analytical expressions, however, may be readily extended from the two layer case treated above. To derive first these general formulae we may suppose that the potential distribution on the earth's surface has again been found as an integral over Bessel functions and may be expressed in the units of Eq. (1a) as:

$$\Phi=1/\rho+2\int_0^\infty f(\alpha)J_0(2\rho\alpha)d\alpha, \qquad (19)$$

where $f(\alpha)$, in the case of an n-layer earth is the ratio of two determinants of order $n+1$ and contains as parameters the conductivities and depths of the n layers. For large values of α, $f(\alpha)\sim e^{-2\alpha}$, which insures the convergence of the integral in Eq. (19).

We may now obtain the formal expansion of $\Phi-1/\rho$ as a power series in ρ by again replacing $J_0(2\rho\alpha)$ by its power series. We have then as the expansion to be used for small values of ρ:

[13] Cf. Trans. Amer. Inst. Min. Met. Engr., "Geophysical Prospecting," 1932, p. 440.

$$\Phi=\frac{1}{\rho}+2\sum_0^\infty \frac{(-1)^m\rho^{2m}}{\Gamma^2(m+1)}\int_0^\infty \alpha^{2m}f(\alpha)d\alpha. \quad (20)$$

For large values of ρ we develop a general theorem for the asymptotic expansion of integrals of the type occurring in Eq. (19), which is a natural extension of the particular development used in the case of the two layer earth. Thus we suppose that $f(\alpha)$ can be expanded in a series of partial fractions in the form:

$$f(\alpha)=f(0)+\sum b_n\{1/(\alpha-\alpha_n)+1/\alpha_n\}, \quad (21)^{14}$$

where $\alpha=\alpha_n$ are simple poles of $f(\alpha)$ with residues b_n. Eq. (19) then takes the form:

$$\Phi=\frac{1}{\rho}\left\{1+f(0)+\sum\frac{b_n}{\alpha_n}\right\}+2\sum b_n\int_0^\infty \frac{J_0(2\rho\alpha)d\alpha}{\alpha-\alpha_n}.$$

We now observe that:

$$\int_0^\infty \frac{J_0(2\rho\alpha)d\alpha}{\alpha+k}=\frac{\pi}{2}\{\overline{H}_0(2\rho k)-Y_0(2\rho k)\}, \quad (22)$$

where $\overline{H}_0$ is again the Struve function we met in Eq. (10a). Φ becomes, then:

$$\Phi=(1/\rho)\{1+f(0)+\sum b_n/\alpha_n\}+\pi\sum b_n\{\overline{H}_0(-2\rho\alpha_n)-Y_0(-2\rho\alpha_n)\}. \quad (23)$$

Since we are interested mainly in the asymptotic expansion of Φ with respect to ρ we may apply again Eq. (13) to obtain:

$$\Phi=\frac{1}{\rho}\{1+f(0)+\sum b_n/\alpha_n\}+\frac{1}{\pi}\sum b_n\sum_0^p m\frac{(-1)\Gamma^2(m+\frac{1}{2})}{(-\rho\alpha_n)^{2m+1}}+0(\rho^{-2p-1}).$$

Now from Eq. (21), it follows that for $m>0$, $f^{2m}(0)=\Gamma(2m+1)\sum b_n/(-\alpha_n)^{2m+1}$.

We therefore have finally:

$$\Phi=\frac{1}{\rho}+\frac{1}{\pi}\sum_0^p m\frac{(-1)^m\Gamma^2(m+\frac{1}{2})f^{2m}(0)}{\Gamma(2m+1)\rho^{2m+1}}+0(\rho^{-2p-1}). \quad (24)$$

Since Eq. (24) involves only differentiations of the function f it will not be difficult to apply even to complex forms for f. Eq. (20), on the other hand, involves the evaluation of a series of definite integrals which in general may be as difficult to evaluate as the single integral of Eq. (19). For small values of ρ it will therefore be necessary to generalize the method used in the case of the two layer earth. Although this method was essentially equivalent to summing the power series expansions of the individual image potentials, it is more convenient to derive the general expressions for the terms than to use the first few series of images already listed by Hummel,[3] for a three layer earth.

B. The three layer earth

For a three layer earth the function f may be written in the form[15]

$$\left.\begin{aligned} &f(\alpha)=2(N_0+k_3N_1)/(\Delta_0+k_3\Delta_1);\\ &N_0=k_2e^{-2\alpha};\quad N_1=e^{-2\alpha h};\quad \Delta_0=1-k_2e^{-2\alpha};\quad \Delta_1=e^{-2\alpha h}(-1+k_2e^{2\alpha})\\ &k_2=(\sigma_1-\sigma_2)/(\sigma_1+\sigma_2);\quad k_3=(\sigma_2-\sigma_3)/(\sigma_2+\sigma_3);\quad h=h_2/h_1>1. \end{aligned}\right\} \quad (25)$$

where:

The general evaluation of the coefficients of ρ^{2m} in Eq. (20) with the $f(\alpha)$ of Eq. (25) is unfortunately rather difficult. One can in a formal manner expand $f(\alpha)$ as:

$$f(\alpha)=\frac{2(N_0+k_3N_1)}{\Delta_0}\sum_0^\infty n(-1)^nk_3^n\left(\frac{\Delta_1}{\Delta_0}\right)^n,$$

[14] Cf. Whittaker and Watson, *Modern Analysis*, p. 134. In the appendix we shall give a more general proof applying not only to functions $f(\alpha)$ as $e^{-\beta\alpha}$ which do not permit the partial fraction expansion of Eq. (21), but also the expansions corresponding to Bessel functions of the second and third kinds and to functions of non-zero order.

[15] Stefanesco and Schumberger, reference 4.

in which the term independent of k_3 will give the potential due to a two layer earth ($k_3=0$, $\sigma_3=\sigma_2$). The higher order terms can then be expressed as derivatives of this two layer potential with respect to k_2. In this way one may obtain a power series expansion in ρ of the series of Hummel. The coefficients of this series, however, will themselves be double series with respect to powers of k_2 and k_3, with unsatisfactory convergence characteristics. It will therefore be more convenient to treat the potential for small values of ρ separately for special integral values of h, but by a method which not only leads to more satisfactory series but which also permits an extension to rational values of h.

On the other hand, with regard to the series of Eq. (24) for large values of ρ, the general case offers no difficulties in principle, although the successive differentiations of $f(\alpha)$ become rather lengthy. Thus, putting in the value of $f(\alpha)$ as given by Eq. (25) we have for the first two terms:

$$\Phi\rho=\frac{\sigma_1}{\sigma_3}\left[1-\frac{(\sigma_2^2-\sigma_3^2)\{\sigma_1-\sigma_2+\sigma_2 h\}^2+\sigma_3^2(\sigma_1^2-\sigma_2^2)}{4\sigma_2^2\sigma_3^2\rho^2}\right], \tag{26}$$

where it is to be recalled that $h=h_2/h_1$.

As we should expect, if $\sigma_2=\sigma_3$ or $\sigma_1=\sigma_2$, Eq. (26) reduces to Eq. (16) which we derived for the two layer earth. For very large distances $\Phi\rho$ approaches the value σ_1/σ_3 and is independent of the conductivity of the second layer. Thus if $\sigma_1=\sigma_3$, $\Phi\rho$ has, for large ρ, the same value as in a homogeneous earth. Its approach, however, to the value 1 does depend on σ_2, coming down from higher values if $\sigma_2<\sigma_1$, and up from lower values if $\sigma_2>\sigma_1$. On the other hand, for smaller distances the second layer does come into play and its effect increases rapidly with its thickness, as is clear from the second term in Eq. (26).

We shall now return to the potential distribution for small values of ρ for two special values of h.

Power series expansions for special values of h.

$h=2$. When the thickness of the second layer is exactly equal to that of the upper layer the $f(\alpha)$ as given by Eq. (25) can be re-expressed in a form which permits an application of the method used for a two layer earth. Thus we have

$$f(\alpha)=\frac{2e^{-2\alpha}(k_2+k_3e^{-2\alpha})}{1-k_2(1-k_3)e^{-2\alpha}-k_3e^{-4\alpha}}=\frac{k_3e^{-3\alpha}+k_2e^{-\alpha}}{[k_2^2(1-k_3)^2+4k_3]^{\frac{1}{2}}}\left\{\frac{e^{-\gamma_1}}{\sinh(\alpha+\gamma_1)}-\frac{e^{-\gamma_2}}{\sinh(\alpha+\gamma_2)}\right\}, \tag{27}$$

where:

$$\left.\begin{aligned}2k_3e^{2\gamma_1}&=-k_2(1-k_3)+[k_2^2(1-k_3)^2+4k_3]^{\frac{1}{2}}\equiv 2k_3/s_1,\\ 2k_3e^{2\gamma_2}&=-k_2(1-k_3)-[k_2^2(1-k_3)^2+4k_3]^{\frac{1}{2}}\equiv 2k_3/s_2.\end{aligned}\right\} \tag{27a}$$

Carrying through now the same expansions and integrations as in Section A of Part I, it is found, by means of Eq. (19), that for the present case:

$$\left.\begin{aligned}\Phi=\frac{1}{\rho}+\frac{2}{[k_2^2(1-k_3)^2+4k_3]^{\frac{1}{2}}}\Bigg[&k_2\log\frac{1-s_2}{1-s_1}+\frac{k_3}{s_2}\log(1-s_2)-\frac{k_3}{s_1}\log(1-s_1)\\ &+\sum_1^\infty m(-1)^m c_m\rho^{2m}\sum_1^\infty n(s_1^n-s_2^n)\left\{\frac{k_2}{n^{2m+1}}+\frac{k_3}{(n+1)^{2m+1}}\right\}\Bigg].\end{aligned}\right\} \tag{28}$$

If $k_3=0(\sigma_3=\sigma_2)$, Eq. (28) easily reduces to the Φ of Eq. (5) for a two layer earth; and if $k_2=0(\sigma_2=\sigma_1)$, Eq. (5) is again found with ρ changed to $\rho/2$ and a factor of 2 in Φ.

If the lower layer has an infinite resistivity ($\sigma_3=0$; $k_3=+1$), Eq. (27) gives an infinite constant in addition to the series, as is to be expected since $f(\alpha)$ has a pole at $\alpha=0$ if $k_3=1$. Eq. (28) reduces

then to:

$$\Phi(k_3=1,\ \sigma_3=0)=\frac{1}{\rho}+\left[(k_2-1)\log 2-(k_2+1)\lim_{s_1\to 1}\log(1-s_1)\right.$$
$$\left.+2\sum_1^\infty(-1)^m c_m\rho^{2m}\sum_{\text{odd}}n\left(\frac{k_2}{n^{2m+1}}+\frac{1}{(n+1)^{2m+1}}\right)\right]. \tag{28a}$$

In using these formulae the procedure followed in Part I may be applied in separating out and summing the terms for $n=1$, and 2, thus increasing the radius of convergence of the series. Since $|s_1|$ and $|s_2|$ are less than 1, the same function $f_m(k)$ occurring in Eq. (6) can be used with Eq. (28) after separating out the $n=1$, 2 terms, except that the arguments will be s_1 and s_2 instead of the k of Eq. (6).

For large values of ρ, the more general Eq. (26) may be used with h set equal to 2.

$h=3$. When the second layer is two times as thick as the upper layer the analysis can again be carried through in detail, although it will be convenient to make it somewhat more formal than in the case of $h=2$. Thus we shall suppose that the denominator of $f(\alpha)$ has been factored, so that $f(\alpha)$ can be rewritten as:

$$f(\alpha)=\frac{-2e^{-2\alpha}(k_2/k_3+e^{-4\alpha})}{(e^{-2\alpha}-e^{2\gamma_1})(e^{-2\alpha}-e^{2\gamma_2})(e^{-2\alpha}-e^{2\gamma_3})}$$
$$=e^{-\alpha}(k_2+k_3e^{-4\alpha})\left\{\frac{s_1e^{-\gamma_1}/(s_2-s_1)(s_3-s_1)}{\sinh(\alpha+\gamma_1)}+\frac{s_2e^{-\gamma_2}/(s_1-s_2)(s_3-s_2)}{\sinh(\alpha+\gamma_2)}+\frac{s_3e^{-\gamma_3}/(s_1-s_3)(s_2-s_3)}{\sinh(\alpha+\gamma_3)}\right\}, \tag{29}$$

where

$$e^{-2\gamma_1}=s_1;\quad e^{-2\gamma_2}=s_2;\quad e^{-2\gamma_3}=s_3. \tag{29a}$$

Again applying the method of Section A, Part I we find:

$$\Phi=\frac{1}{\rho}+\frac{2}{(s_2-s_1)(s_3-s_1)(s_3-s_2)}\sum_0^\infty m(-1)^m c_m\rho^{2m}\sum_1^\infty n\left\{\frac{k_2}{n^{2m+1}}+\frac{k_3}{(n+2)^{2m+1}}\right\}$$
$$\cdot\{s_1{}^{n+1}(s_3-s_2)+s_2{}^{n+1}(s_1-s_3)+s_3{}^{n+1}(s_2-s_1)\}. \tag{30}$$

Here, too, the constant terms for $m=0$ and those for $n=1$, 2, may be taken out and summed separately and the remaining sums with respect to n expressed in terms of $f_m(s)$. Although s_1, s_2, s_3 cannot be expressed in simple explicit forms, they may be readily obtained in any particular case as the reciprocals of the roots of the trinomial denominator of $f(\alpha)$ set equal to zero. And again Φ for large ρ may be found by means of Eq. (26) with h set equal to 3.

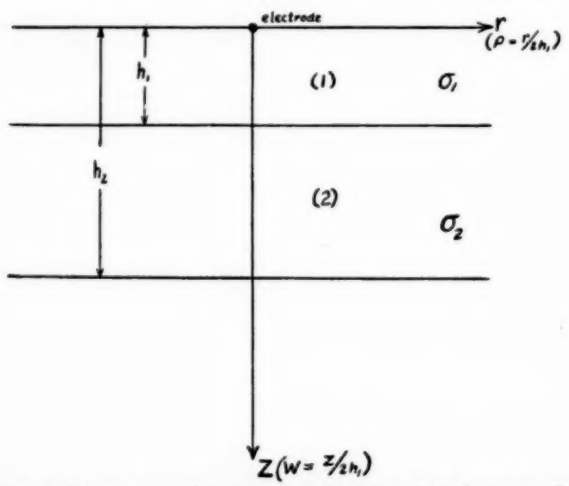

FIG. 4. Diagrammatic representation of a three layer earth.

It may be noted that insofar as the roots of any polynomial may be found graphically the above method may be extended directly to systems where h is any rational fraction, although it will of course become increasingly complex as the degree of the polynomial increases.

Lower layer of zero conductivity

When the lower is of zero conductivity ($\sigma_3=0$, $k_3=+1$) the potentials diverge, as in the case

of the two layer earth. This may be seen on the one hand from the asymptotic expansion of Eq. (26), which becomes infinite when $\sigma_3=0$, or from the form of $f(\alpha)$ of Eq. (25), which has a pole at $\alpha=0$ for $k_3=+1$.

For small values of ρ we have seen how the divergence of Φ may be separated out into a logarithmic term. Thus for $h=2$, Eq. (28a) gives the infinite part of Φ as $-(1+k_2)\lim_{s_1\to 1}\log(1-s_1)$. And similarly in the case $h=3$, it may be shown by summing in Eq. (30) the terms with $m=0$ and taking s_1 as the reciprocal of the root of value unity, that the infinite term of Φ is:

$$\frac{-2(1+k_2)}{3-k_2}\lim_{s_1\to 1}\log(1-s_1).$$

For large values of ρ we must find a new asymptotic expansion, as Eq. (26) diverges everywhere for $\sigma_3=0$. The situation is similar to that encountered in the case of Eq. (16) for a two layer earth, and may be treated in the same way.

Thus, for $h=2$ we see from Eq. (25) that the poles of the two parts of $f(\alpha)$ are:

$$\alpha_n=n\pi i-\gamma_1;\quad n\pi i-\gamma_2 \tag{31}$$

with residues:

$$b_n=\frac{(-1)^n e^{-\gamma_1}(k_3e^{-3\alpha_n}+k_2e^{-\alpha_n})}{[k_2^2(1-k_3)^2+4k_3]^{\frac{1}{2}}};\quad \frac{-(-1)^n e^{-\gamma_2}(k_3e^{-3\alpha_n}+k_2e^{-\alpha_n})}{[k_2^2(1-k_3)^2+4k_3]^{\frac{1}{2}}}. \tag{31a}$$

Noting that for $k_3=1$, $\gamma_1=0$, $\gamma_2=\pi i/2$, and that for each set, $b_n=b_{-n}=b_0$, it is readily found that:

$$\lim_{(k_3\to 1)}\{1+f(0)+\sum b_n/\alpha_n\}=0.$$

Applying now Eqs. (23) and (17) we have finally,

$$\left.\begin{aligned}\lim_{\sigma_3\to 0}\Phi(h=2)=(1+k_2)\left\{-\lim_{\gamma_1\to 0}\log 2\gamma_1-0.5772+\log 2/\rho\right\}\\ +2\sum_1^\infty nK_0(n\pi\rho)+2k_2\sum_1^\infty n(-1)^nK_0(n\pi\rho).\end{aligned}\right\} \tag{32}$$

For $h=3$, we return to Eq. (29) and note that for $k_3=1$:

$$\left.\begin{aligned}\gamma_1=0;\quad \gamma_2=-i\theta/2;\quad \gamma_3=i\theta/2;\quad \cos\theta=(k_2-1)/2\\ b_n(\gamma_1)=(1+k_2)/(3-k_2);\quad b_n(\gamma_2)=b_n(\gamma_3)=(1-k_2)/(3-k_2)\end{aligned}\right\} \tag{33}$$

so that, again:

$$\lim_{k_3\to 1}\{1+f(0)+\sum b_n/\alpha_n\}=0.$$

Applying once more Eqs. (23) and (17) we finally find that

$$\left.\begin{aligned}\lim_{\sigma_3\to 0}\Phi(h=3)=[2(1+k_2)/(3-k_2)]\{-\lim_{\gamma_1\to 0}\log 2\gamma_1-0.5772+\log 2/\rho+2\sum_1^\infty nK_0(2n\pi\rho)\}\\ +[4(1-k_2)/(3-k_2)]\{\sum_0^\infty nK_0(2n\pi\rho+\theta\rho)+\sum_1^\infty nK_0(2n\pi\rho-\theta\rho)\}\end{aligned}\right\}. \tag{34}$$

Similarly, for $h=4$, it may be shown without difficulty that for $\sigma_3=0(k_3=1)$ the poles of $f(\alpha)$ and their residues are:

$$\left.\begin{aligned}\alpha_n=n\pi i+0;\quad n\pi i-\pi i/2;\quad n\pi i-i\theta/2;\quad n\pi i+i\theta/2\\ b_n=\frac{1+k_2}{2(2-k_2)};\quad \frac{1-k_2}{2(2+k_2)};\quad \frac{1-k_2^2}{4-k_2^2};\quad \frac{1-k_2^2}{4-k_2^2};\quad \cos\theta=\frac{k_2}{2}\end{aligned}\right\}. \tag{35}$$

Putting these in Eq. (23) and making use of Eq. (17) we find that:

$$\lim_{\sigma_2\to 0}\Phi(h=4)=[(1+k_2)/(2-k_2)]\left\{-\lim_{\gamma_1\to 0}\log 2\gamma_1-0.5772+\log 2/\rho+2\sum_1^\infty nK_0(2n\pi\rho)\right\}+[2(1-k_2)/(2+k_2)]\sum_0^\infty nK_0((2n+1)\pi\rho)+[4(1-k_2^2)/(4-k_2^2)]\left\{\sum_0^\infty nK_0(2n\pi\rho+\theta\rho)+\sum_1^\infty nK_0(2n\pi\rho-\theta\rho)\right\}\Bigg\}. \quad (36)$$

Before presenting the analogous formulae for the case of a lower layer of infinite conductivity ($\sigma_3=\infty$, $k_3=-1$) it may be observed that Eqs. (32), (34) and (36) all reduce, as they should, to Eq. (18), derived for a two layer earth, when k_2 is set equal to $1(\sigma_2=0)$, or $0(\sigma_2=\sigma_1)$.

Lower layer of infinite conductivity

When the lowest layer is of zero resistance closed series of Hankel functions may again be obtained. As in the corresponding case for a two layer earth (cf. Eq. (11c)), the series are strictly convergent and involve no logarithmic terms or infinite constants. The method of derivation, however, is identical with that for $\sigma_3=0$ and will be only briefly indicated.

Thus for $h=2$, the poles and residues of $f(\alpha)$ are:

$$\left.\begin{array}{l}\alpha_n=n\pi i+i\theta/2;\quad n\pi i-i\theta/2;\quad \cos\theta=k_2\\ b_n=\tfrac{1}{2};\quad \tfrac{1}{2}.\quad 1+f(0)+\sum b_n/\alpha_n=0\end{array}\right\}. \quad (37)$$

By using once more the general series of Eq. (23) and reducing by means of Eq. (17), it is found that:

$$\Phi(\sigma_3=\infty;\ h=2)=2\sum_0^\infty nK_0(2n\pi\rho+\theta\rho)+2\sum_1^\infty nK_0(2n\pi\rho-\theta\rho). \quad (38)$$

For $h=3$, we have similarly:

$$\left.\begin{array}{l}\alpha_n=(2n+1)\pi i/2;\quad n\pi i-i\theta/2;\quad n\pi i+i\theta/2;\quad \cos\theta=(1+k_2)/2\\ b_n=(1-k_2)/(3+k_2);\quad (1+k_2)/(3+k_2);\quad (1+k_2)/(3+k_2);\quad 1+f(0)+\sum b_n/\alpha_n=0\end{array}\right\} \quad (39)$$

so that:

$$\Phi(\sigma_3=\infty,\ h=3)=\frac{4(1-k_2)}{3+k_2}\sum_0^\infty nK_0((2n+1)\pi\rho)+\frac{4(1+k_2)}{3+k_2}\left\{\sum_0^\infty nK_0(2n\pi\rho+\theta\rho)+\sum_1^\infty nK_0(2n\pi\rho-\theta\rho)\right\}. \quad (40)$$

Finally, for the case $h=4$, we have:

$$\left.\begin{array}{l}\alpha_n=n\pi i-i\theta_1/2;\quad n\pi i+i\theta_1/2;\quad n\pi i-i\theta_2/2;\quad n\pi i+i\theta_2/2,\\ \qquad \cos\theta_1=\{k_2+(k_2^2+8)^{\frac{1}{2}}\}/4;\quad \cos\theta_2=\{k_2-(k_2^2+8)^{\frac{1}{2}}\}/4,\\ b_n=\dfrac{3k_2+(k_2^2+8)^{\frac{1}{2}}}{4(k_2^2+8)^{\frac{1}{2}}};\quad \dfrac{3k_2+(k_2^2+8)^{\frac{1}{2}}}{4(k_2^2+8)^{\frac{1}{2}}};\quad \dfrac{-3k_2+(k_2^2+8)^{\frac{1}{2}}}{4(k_2^2+8)^{\frac{1}{2}}};\quad \dfrac{-3k_2+(k_2^2+8)^{\frac{1}{2}}}{4(k_2^2+8)^{\frac{1}{2}}},\end{array}\right\} \quad (41)$$

so that: $1+f(0)+\sum b_n/\alpha_n=0$

and

$$\left.\begin{aligned}\Phi(\sigma_3=\infty\,;\,h=4)=&\frac{3k_2+(k_2^2+8)^{\frac{1}{2}}}{(k_2^2+8)^{\frac{1}{2}}}\left\{\sum_0^\infty nK_0(2n\pi\rho+\theta_1\rho)+\sum_1^\infty nK_0(2n\pi\rho-\theta_1\rho)\right\}\\&+\frac{-3k_2+(k_2^2+8)^{\frac{1}{2}}}{(k_2^2+8)^{\frac{1}{2}}}\left\{\sum_0^\infty nK_0(2n\pi\rho+\theta_2\rho)+\sum_1^\infty nK_0(2n\pi\rho-\theta_2\rho)\right\}.\end{aligned}\right\}\tag{42}$$

Again it may be observed that Eqs. (38), (40) and (42) reduce to that for the two layer potential (cf. e.g., (11c)) both when k_2 is set equal to $-1(\sigma_2=\infty)$ or $0(\sigma_2=\sigma_1)$.

Numerical treatment

To illustrate the analytical results obtained above the computations for a number of cases for which numerical results have as yet not been given in the literature have been carried through in detail and will be presented in graphical form.

In Fig. 5 curves are given for $\Phi\rho$ for the cases of a slab of thickness equal to that of the top layer ($h=2$) immersed in an otherwise homogeneous earth ($\sigma_1=\sigma_3$). The two cases are for $\sigma_1=5\sigma_2$ and $\sigma_2=5\sigma_1$. As already suggested in our discussion of Eq. (26), $\Phi\rho$ for these cases approaches 1 for large ρ, with $\Phi\rho>1$ for $\sigma_1=5\sigma_2$, and $\Phi\rho<1$ for $\sigma_2=5\sigma_1$. For small ρ Eq. (28) was used with the terms for $n=1$, 2 summed separately. In the case $\sigma_2=5\sigma_1$, s_1 and s_2 were real and the resulting sums for n were expressed as $f_m(s)$. In the case $\sigma_1=5\sigma_2$, s_1, s_2 were complex but the series reduced quite simply, although the $f_m(s)$ could not be used. In both cases only four terms in the series with respect to m gave high accuracies even for $\rho=2.5$. For large ρ the extensions of Eq. (26) were used. The higher derivatives indicated in Eq. (24) were most easily derived by expanding separately the numerators and denominators of $f(\alpha)$ in

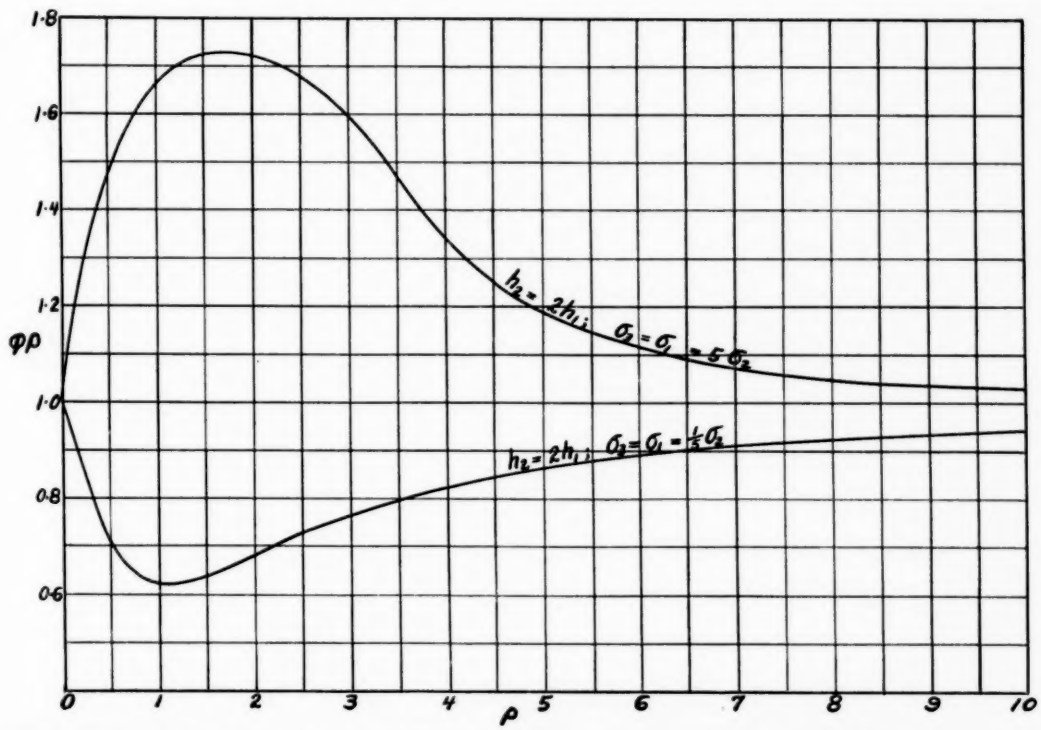

FIG. 5. Surface potentials for the case of a slab of thickness equal to that of the top layer, immersed in an otherwise homogeneous earth.

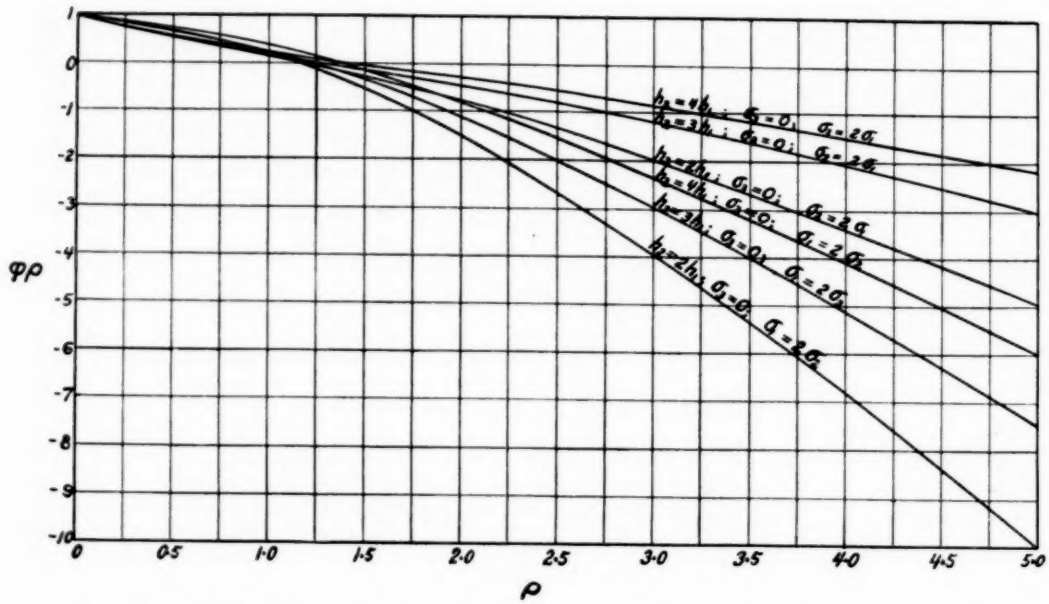

FIG. 6. Surface potentials for a three layer earth in which the lowest layer has a zero conductivity and the conductivity ratios of the two upper layers are 1 : 2 and 2 : 1. h_1 = thickness of surface layer; $h_2 - h_1$ = thickness of second layer; ρ = (radial distance from electrode)/$2h_1$.

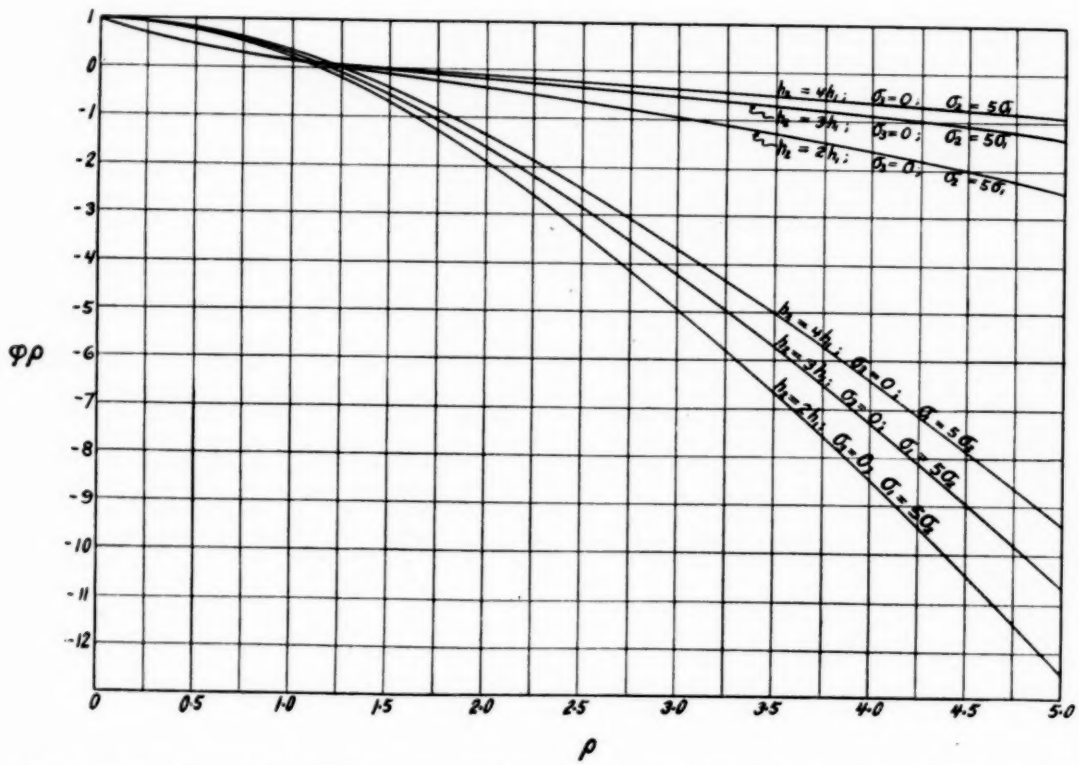

FIG. 7. Surface potentials for a three layer earth in which the lowest layer has a zero conductivity and the conductivity ratios of the two upper layers are 1 : 5 and 5 : 1.

powers of α and then getting the coefficients of α^{2m} in the ratio by well-known algebraic rules. In the case of $\sigma_2=5\sigma_1$, the convergence of the asymptotic expansion was made very rapid by using the analogue of Eq. (15a), i.e.:

$$\Phi=\frac{1}{\rho}+\pi b_0\{\bar{H}_0(-2\rho\alpha_0)-Y_0(-2\rho\alpha_0)\}+\frac{1}{\pi}\sum_0^p m\frac{(-1)^m\Gamma^2(m+\tfrac{1}{2})}{\Gamma(2m+1)\rho^{2m+1}}\left\{f^{2m}(0)+\frac{b_0\Gamma(2m+1)}{\alpha_0{}^{2m+1}}\right\} \quad (43)$$

where the notation is that of Eq. (23), α_0 being the pole of $f(\alpha)$ of smallest absolute value.

Cases in which the lower layer is of zero conductivity ($\sigma_3=0$) are illustrated in Figs. 6 and 7, for middle layers of thickness, 1, 2 and 3 times that of the upper layer. Eqs. (32)–(36) were used in computing these. The inflections in the curves for $\sigma_2>\sigma_1$ and the almost exact overlapping of all the curves for $\rho<1$ may be noted. Of more interest, however, from the analytical point of view is the fact that the equations (32)–(36) (as well as Eqs. (38)–(42) for $\sigma_3=\infty$) are *rigorous* expressions for Φ and furthermore converge so rapidly that even for $\rho=0.25$ less than eight terms in the series over K_0 will give errors less than 0.05 percent. For $\rho\geq 1$ only two terms give equally high accuracies. As, by definition, $\Phi\rho=1$ for $\rho=0$, these series were very satisfactory for numerical treatment over the complete range of ρ.

Similar curves for $\sigma_3=\infty$ are given in Figs. 8 and 9. Of particular interest here is the fact that although all the curves approach 0 as ρ becomes large the curves for $\sigma_2>\sigma_1$ lie much closer together, just as in the case of the two layer earth (cf. Fig. 3). As to the convergence of the series, they are just as satisfactory as those for $\sigma_3=0$.

As a single generalization of the detailed analysis developed here for two and three layer earths, we shall simply mention that since for an n layered earth $f(0)=(\sigma_1-\sigma_n)/\sigma_n$, the potential, by Eq. (24), for an n layered earth will approach the value

$$\Phi=\sigma_1/\sigma_n\rho \quad (44)$$

as ρ becomes very large. Thus, in general, as already suggested by others, the potential at large distances from the electrode is determined only by the topmost and deepest layers. And finally it may be noted that the asymptotic expansions developed here can be applied to continuously varying conductivities as well as those varying discontinuously.

In concluding, the author wishes to mention that after all the analysis of the present paper had been developed and written up, and while the author was waiting for the completion of the numerical work, a paper by L. V. King on the same problem appeared in the February 1st number of the Royal Society Proceedings. Although King's analysis in Sections 7–11 is almost identical in many respects with that developed by the author there are after all enough differences in the final results that it has seemed best to leave the author's original manuscript unchanged. Among the results developed by the author and not given by King are: (1), detailed discussion of the power series for small values of ρ (Eqs. (6), (20), (28), (30)); (2), expressions valid when the electrode is *not* on the surface and for potentials *below* the surface (Eqs. (8), (11), (12)); (3), the closed expansion for Φ in terms of Struve's function, which is very useful in getting the potentials for $\sigma_3=0$, ∞, as well as for evaluating, in general, a large class of Bessel function integrals (Eq. (23)); (4), explicit expansions for the potential for a three layer earth (Eqs. (34)–(43)); (5), explicit expressions for the asymptotic expansions in terms of the conductivities (Eqs. (16), (26)); (6), thirty numerical cases represented in graphical form; and (7), a general proof of the expansion of Eq. (24) which permits the method to be applied to continuously varying conductivities (Appendix). On the other hand it should at the same time be mentioned that King does include discussions of field graphs and alternating current problems, which have not been considered in the present paper.

The writer is indebted to Professor Harry Bateman for helpful suggestions with respect to some of his earlier work on this problem, to Mr. R. D. Wyckoff, Dr. P. D. Foote and Dr. E. A. Eckhardt for permission to publish this work, and to Mr. M. W. Meres for the painstaking care with which he has computed and plotted the data for the various figures of this paper.

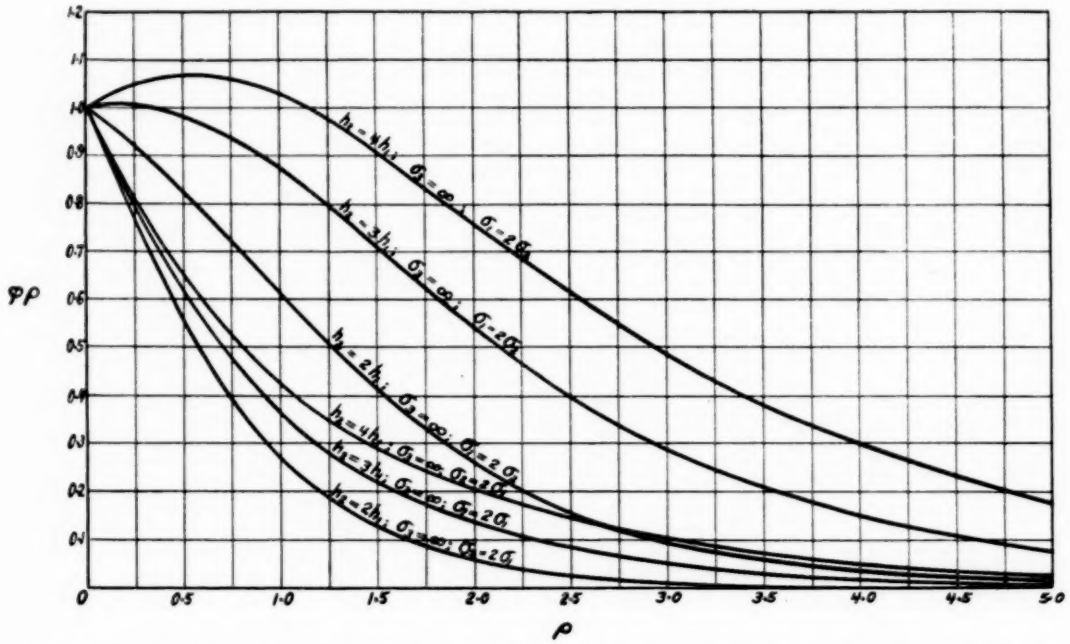

FIG. 8. Surface potentials for a three layer earth in which the lowest layer has an infinite conductivity and the conductivity ratios of the two upper layers are 1 : 2 and 2 : 1.

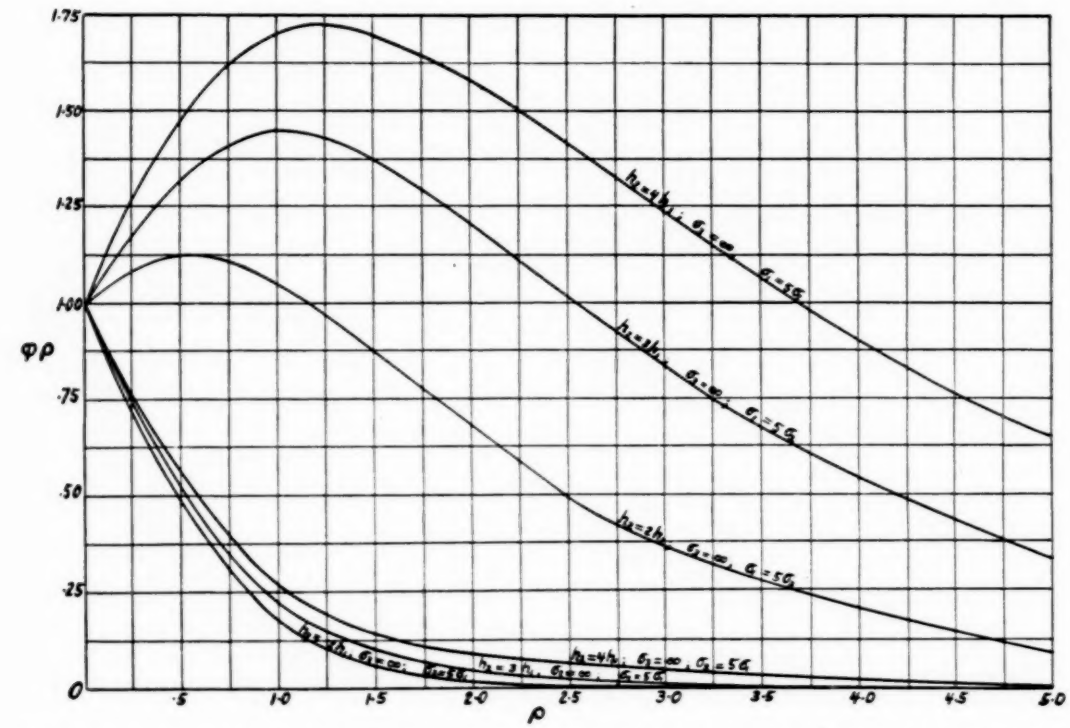

FIG. 9. Surface potentials for a three layer earth in which the lowest layer has an infinite conductivity and the conductivity ratios of the two upper layers are 1 : 5 and 5 : 1.

Appendix

As may be readily verified by trial, Eq. (24) is valid not only for such functions $f(\alpha)$ as permit an expansion in partial fractions, but also for such functions as $e^{-\beta\alpha}$, $e^{-\beta\alpha^2}$ or $J_0(\alpha)$. That it has a more general validity—although Eq. (23) applies only to functions with partial fraction expansions—may be proved as follows.

By Watson, p. 170, we have for: $-\frac{1}{2}<R(\nu)<\frac{1}{2}$

$$\alpha^{\nu}J_{\nu}(\alpha\rho)=\frac{2^{\nu+1}}{\rho^{\nu}\Gamma(\frac{1}{2}-\nu)\Gamma(\frac{1}{2})}\int_1^{\infty}\frac{\sin\alpha\rho t}{(t^2-1)^{\nu+\frac{1}{2}}}dt \tag{45}$$

$$\therefore\quad P_{\nu}(\rho)=\int_0^{\infty}\alpha^{\nu}J_{\nu}(\alpha\rho)f(\alpha)d\alpha=\frac{2^{\nu+1}}{\rho^{\nu}\Gamma(\frac{1}{2}-\nu)\Gamma(\frac{1}{2})}\int_1^{\infty}\frac{dt}{(t^2-1)^{\nu+\frac{1}{2}}}\int_0^{\infty}f(\alpha)\sin\alpha\rho t d\alpha.$$

Now the second integral has the asymptotic expansion (successive integrations by parts):

$$\int_0^{\infty}f(\alpha)\sin\alpha\rho t d\alpha=\sum_0^{\infty}\frac{(-1)^m f^{2m}(0)}{(\rho t)^{2m+1}}. \tag{46}$$

Putting this in $P_{\nu}(\rho)$ and integrating with respect to t, we find:

$$P_{\nu}(\rho)=\frac{2^{\nu}}{\pi^{\frac{1}{2}}\rho^{\nu}}\sum_0^{\infty}m\frac{(-1)^m\Gamma(m+\nu+\frac{1}{2})f^{2m}(0)}{\Gamma(m+1)\rho^{2m+1}}, \tag{47}$$

which for $\nu=0$ is identical with Eq. (24), taking into account the difference between the definitions of ρ and $f(\alpha)$, here and in Eq. (24).

Noting similarly that for $-\frac{1}{2}<R(\nu)<\frac{1}{2}$

$$\alpha^{\nu}Y_{\nu}(\alpha\rho)=\frac{-2^{\nu+1}}{\rho^{\nu}\Gamma(\frac{1}{2}-\nu)\Gamma(\frac{1}{2})}\int_1^{\infty}\frac{\cos\alpha\rho t}{(t^2-1)^{\nu+\frac{1}{2}}}dt$$

and that:

$$\int_0^{\infty}f(\alpha)\cos\alpha\rho t d\alpha=\sum_0^{\infty}\frac{(-1)^{m+1}f^{2m+1}(0)}{(\rho t)^{2m+2}}$$

we get:

$$Q_{\nu}(\rho)=\int_0^{\infty}\alpha^{\nu}Y_{\nu}(\alpha\rho)f(\alpha)d\alpha$$

$$=\frac{2^{\nu}}{\pi^{\frac{1}{2}}\rho^{\nu+1}}\sum_0^{\infty}m\frac{(-1)^m\Gamma(m+\nu+1)f^{2m+1}(0)}{\Gamma(m+\frac{3}{2})\rho^{2m+1}}. \tag{48}$$

And finally, since for $-\frac{1}{2}<R(\nu)<1$

$$\alpha^{-\nu}K_{\nu}(\alpha\rho)=\frac{\Gamma(\frac{1}{2})\rho^{\nu}}{2^{\nu}\Gamma(\nu+\frac{1}{2})}\int_1^{\infty}e^{-\alpha\rho t}(t^2-1)^{\nu-\frac{1}{2}}dt$$

and

$$\int_0^{\infty}e^{-\alpha\rho t}f(\alpha)d\alpha=\sum_0^{\infty}\frac{f^m(0)}{(\rho t)^{m+1}}$$

we get:

$$S_{\nu}(\rho)=\int_0^{\infty}\alpha^{-\nu}K_{\nu}(\alpha\rho)f(\alpha)d\alpha$$

$$=\frac{\pi^{\frac{1}{2}}\rho^{\nu}}{2\nu+1}\sum_0^{\infty}m\frac{\Gamma((m+1)/2-\nu)f^m(0)}{\Gamma(m/2+1)\rho^{m+1}}. \tag{49}$$

When $f(\alpha)$ is odd or even Eqs. (47) and (48), respectively, break down. As already seen in the text this is due to the fact that in these cases the integrals P and Q have *exponentially decreasing* asymptotic expansions. This may again be proved generally by considering the functions

$$I=\int_0^{\infty}f(\alpha)\begin{matrix}\sin\alpha\rho t\\ \cos\alpha\rho t\end{matrix}d\alpha$$

as $f(\alpha)$ is odd or even. Thus, if $f(\alpha)$ is odd and $f(\alpha)\sim 1/\alpha^{(1+\epsilon)}$ for $|\alpha|\sim\infty$ a contour integration of the integral shows that

$$I=\frac{\pi}{2}\sum\epsilon_n[\text{res }\{f(\alpha)e^{i\rho\alpha}\}_{\alpha_n}+\text{res }\{f(\alpha)e^{-i\rho\alpha}\}_{\beta_n}] \tag{50}$$

where α_n are the poles of $f(\alpha)$ in the first quadrant, β_n the poles in the 4th quadrant and $\epsilon_n=2$ if the real parts of (α_n, β_n) are positive and $\epsilon_n=1$ if they are 0. It follows at once that I vanishes exponentially with large ρ, and similarly for the integral with $\cos\alpha\rho t$ if $f(\alpha)$ is even.

The Crystal Structure of Uranium

THOMAS A. WILSON, *Union College, Schenectady, N. Y.*

(Received February 6, 1933)

A method capable of solving x-ray powder photographs derived from crystal structures of low symmetry has been described. By the use of this method, the crystal structure of uranium has been obtained. Uranium crystallizes according to space group C_{2h}^3 of the monoclinic system, with 2 atoms in each crystallographic cell. The dimensions of the cell are: $a=2.829$A, $b=4.887$A, $c=3.308$A. Axial ratios are: 0.5791 : 1 : 0.6771. The x-ray density of uranium is 19.05. The uranium atoms appear to be prolate spheroids with 3.425A as the major axis and 2.826A as the minor axis.

THE crystal structure of uranium has been reported by McLennan and McKay[1] as body-centered cubic, with $a=3.43$ Angstrom units. Knaggs, Karlik and Elam[2] report that a better agreement with the experimental data is afforded with $a=5.50$A. In Wyckoff's compilation[3] of crystal structure data uranium is noted as being not cubic. The spacings observed by McLennan and McKay are in very poor agreement with either of the cubic structures suggested, and their reported spacings do not agree with those observed on his x-ray films by the author. Their procedure of preparing the specimen for analysis is open to question.

Uranium is representative of a large class of substances possessing lower crystal symmetry of which single crystals are either difficult or impossible of preparation. Hence the crystal structure must be determined from an analysis of x-ray photographs obtained by some variety of the powder method. Runge[4] has proposed such a method, which seems to have certain objections preventing its wide adoption. Another method of performing this analysis, and the results obtained by it, form the subjects of this paper.

METHOD OF ANALYSIS OF THE POWDER PHOTOGRAPHS

The method involves the resolution of the simple atomic planes of a crystal structure into the [100], [010] and [001] zonal families, and determining the interplaner relationships necessary in each family to satisfy the observed x-ray reflections.

Consider the nearest equivalent points of some crystal structure, with origin at 0. These points define a parallelopiped called the "simple cell" in this paper. In a homogeneous space lattice, such as the uranium lattice, such a cell contains one equivalent point with the coordinates 000. Hence the structure vector becomes identical with the "loading factor" of Niggli,[5] and no extinctions are produced.

Let $D_1, D_2, \cdots D_n$ be the interplaner spacings obtained for this simple cell by x-ray powder diffraction methods. Then

$$D_1^2 : D_2^2 : D_3^2 : \cdots D_n^2 = 1/F_1 : 1/F_2 : 1/F_3 : \cdots 1/F_n$$

where $F_1, F_2, F_3, \cdots F_n$ represent the F vectors of the reciprocal lattice. By definition,

$$F=K_{11}h^2+K_{22}k^2+K_{33}l^2+2K_{12}hk+2K_{13}hl+2K_{23}kl \quad (1)$$

where h, k and l denote the plane indices. The smallest values of F will generally be obtained when F_1, F_2 and $F_3=K_{11}$, K_{22} and K_{33}, respectively. Hence the largest values of D on the x-ray film will correspond to the face plane spacings of the cell.

[1] McLennan and McKay, Trans. Roy. Soc. (Canada) [III] **24**, 1 (1931).

[2] Knaggs, Karlick and Elam, *Tables of Cubic Crystal Structure*, London, 1932.

[3] Wyckoff, Int. Crit. Tab. **I**, 341 (1926).

[4] Runge, Phys. Zeits. **18**, 509 (1917).

[5] Niggli, Handbuch der experimental Physik **VII**, Part 1, 239 (1928).

Let $e=D_3/D_1=1/F_3^{\frac{1}{2}}=f=D_2/D_1=1/F_2^{\frac{1}{2}}=g=D_1/D_1=1=1/F_1^{\frac{1}{2}}$ define the three vectors e, f and g from 0 which represent the face plane perpendiculars of a cell of such size that the longest perpendicular distance is regarded as unity. (Fig. 1a.) These vectors define a reduced perpendicular lattice.[6] In such a lattice, let $d[100]$, $d[010]$ and $d[001]$ represent the interplaner spacings of the [100], [010] and [001] zones, respectively. These quantities will be defined by the equations:

$$1/d^2[100]=K_{22}'k^2+l^2+2K_{23}'kl \qquad (2)$$

$$1/d^2[010]=K_{11}'h^2+l^2+2K_{13}'hl \qquad (3)$$

$$1/d^2[001]=K_{11}'h^2+K_{22}'k^2+2K_{12}'hk \qquad (4)$$

in which the terms $2K_{23}'$, $2K_{13}'$ and $2K_{12}'$ are still to be determined. Let δ and ϵ refer to the angles shown in the ef plane of Fig. 1a. Then

$$2K_{12}'=\sin^2\delta/\sin^2\epsilon-K_{11}'K_{22}'-1 \qquad (5)$$

and if $K_{11}'K_{22}'=1/m^2$,

$$\tan\epsilon=m\sin\delta/(1-m\cos\delta). \qquad (6)$$

Similar relations exist between $2K_{13}'$, K_{11}', β and θ; and $2K_{23}'$, K_{22}', γ and α.

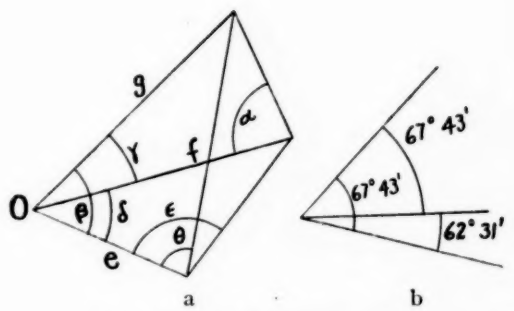

FIG. 1. Reduced lattice of uranium.

Having obtained K_{22}' in Eq. (2) in the manner described, the value of $2K_{23}$ can be obtained if some observed x-ray reflection on the powder photograph is considered as showing the spacing of the (011) plane, equivalent to $d(011)$ of the reduced lattice. This reflection may occasionally be one previously used in connection with the face planes. A short series of increasing F-functions is calculated, and from these the corresponding series of decreasing D-functions. If this series agrees with observed interplaner spacings on the x-ray film, the series is correct. If such agreement is not obtained, another observed x-ray reflection is considered as $D(011)$ and another equation and series are set up. Usually only a trial or two is necessary.

Identical processes are carried out for Eqs. (3) and (4). When these equations have been found, the general equation of the simple cell becomes

$$D=D_1(d[100]+d[010]+d[001]). \qquad (7)$$

As a final check, the interplaner spacings of the other zone families are calculated and compared with the observed x-ray spacings.

If V represents the volume of the simple cell, the expression

$$V=D_1^3[e\cdot(f\times g)] \qquad (8)$$

gives the volume allotted to each atom in the homogeneous space lattice.

PREPARATION OF THE SPECIMEN

The uranium used in this work was in the form of a button. It had been prepared by the method of Goggin, Cronin, Fogg and James.[7] Since filings of uranium catch fire in the air, the x-ray photographs were obtained by reflection from a plane surface of the metal, formed by filing the uranium flat in a hydrogen atmosphere. A bright silvery surface was thus obtained. This surface was not coated to protect it from the oxidizing action of the air. The exposures were obtained in $2\frac{3}{4}$ hours. No visible tarnishing of the metal surface occurred during this period. For additional checks, to show absence of sufficient oxidizing action to affect the x-ray data, photographs were obtained from powder specimens of the uranium oxides supplied by different chemical firms. Films were also prepared from filings of the metal which had been allowed to oxidize in the air at ordinary room temperature. Other films were made from filings heated in the air on a hot plate. None of these films gave x-ray patterns which agreed in any way

[6] Reference 5, p. 108.

[7] Goggin, Cronin, Fogg and James, Ind. Eng. Chem. **18**, 114 (1926).

with those obtained from the filed surface of the metal itself.

The photographs were taken by Dr. W. P. Jesse of the General Electric Research Laboratory. Unfiltered iron radiation was used from a tube operated at 16 m.a. and 38 kv. The radius of the Pye camera was 45.7 mm. The filed surface of the block of uranium was centered in the camera as precisely as possible and was rotated by hand during the exposures.

X-Ray Data

Table I contains the readings made from the second of two exposures. The lines were somewhat clearer on this film, although the lines recorded on the first film agreed in position with those on the second. Readings were made of the positions both right and left of the zero beam as shown in columns 1 and 2 of the table, and the average of the readings was taken as the basis of the calculations (column 3). The wavelengths of the Fe $K\alpha_1$ and the Fe $K\beta$ radiations (1.9323 and 1.7527A, respectively) are those given in Compton.[8] The D and the d values calculated from the x-ray data are tabulated in columns 6 and 7.

TABLE I. *X-ray data. Derivation of the simple uranium cell.*

(1) Readings of film, mm from zero beam Left	(2) Right	(3) Av.	(4) Intensity estimated	(5) Radiation	(6) Observed D-values A	(7) Observed d-values A	(8) Calc. d-values A	(9) Equation	(10) Atomic planes
32.3	32.0	32.2	w	β	2.538				
33.8	33.3	33.5	w	β	2.445				
35.9	35.8	35.8	ms	α	2.535	1.0000	1.0000	10, 11	(100), (010), (001)
36.3	36.3	36.3	w	β	2.261				
37.2	37.1	37.2	ms	α	2.443	0.9637	0.9637	10	(110)
40.6	40.4	40.5	s	α	2.252	0.8884	0.8884	11	(101)
47.3	47.3	47.3	w	β	1.774				
52.9	53.0	53.0	s	α	1.764	0.6959			
56.0	——	56.0	f	β	1.524				
60.5	——	60.5	vf	β	1.427				
63.0	62.9	63.0	ms	α	1.519	0.5992	0.6019 } 0.5984*	11	($\bar{1}01$), ($10\bar{1}$)
				β	1.378		0.5949 }	10	($1\bar{1}0$), ($\bar{1}10$)
68.0	68.0	68.0	w	α	1.427	0.5629	0.5631	10	(120)
70.9	——	70.9	w	α	1.381	0.5448	0.5361	11	(102)
82.0	82.0	82.0	ms	α	1.236	0.4876	0.5000 } 0.4909*	10, 11	(200), (020)
							0.4818 }	10	(220), (002)
91.1	——	91.1	w	α	1.151	0.4540	0.4490	11	(202)
96.7	——	96.7	w	α	1.109	0.4375			
				β	1.006				
117.0		117.0	f	α	1.008	0.3976	0.3926	11	($\bar{2}01$)

s—strong, ms—medium strong, w—weak, f—faint, vf—very faint. Average values shown by *.

The small number of interplaner spacings shown on the film indicate a rather high symmetry in the simple uranium cell. Such symmetry would be imparted to the *ef* plane (Fig. 1a) if $e=f$, or if $\delta=\epsilon$. From previous work on the series of x-ray reflections observed under each of these conditions it seemed more probable that a series in which $e=f$ would fit the observed data. The general equation for the interplaner spacings of the [001] zone then becomes:

$$1/d^2[001]=h^2+k^2+2K_{12}'hk. \qquad (9)$$

Considering $d(110)=0.9637$ in the reduced lattice, $2K_{12}'=-0.9232$, hence Eq. (9) becomes

$$1/d^2[001]=h^2+k^2-0.9232hk. \qquad (10)$$

Comparison of the interplaner spacings calculated by means of Eq. (10) and those observed on the x-ray film is shown in columns 7 and 8 Table I. The atomic planes of the simple cell are listed in column 10. Since in this equation $K_{11}'=K_{22}'=1$, $2K_{12}'=\sin^2\delta/\sin^2\epsilon-2$, $2\epsilon=180-\delta$, from which $\delta=62°\ 31'$.

By applying the same reasoning to the [010] zone, with the value of $d(010)=0.8884$, $2K_{13}=-0.7576$, and Eq. (3) becomes

$$1/d^2[010]=h^2+l^2-0.7576hl. \qquad (11)$$

[8] Compton, *X-rays and Electrons*, p. 396, New York, 1928.

TABLE II. *Comparison of the observed and calculated D values of uranium.*

(1) Calculated values of simple cell Planes	(2) Interplaner spacings (D), in A		(3) Observed values Spacings in A	(4) Intensity	(5) Calculated values of monoclinic cell Planes	(6) Interplaner spacings (D) in A	
(010), (100), (001)	2.535		2.535	ms	(100), (011), (01$\bar{1}$)	2.535	
(110)	2.443		2.443	w	(020)	2.443	
(101), (011)	2.252		2.252	s	(111), (1$\bar{1}$1)	2.281	
(112)	1.772		1.764	s	(12$\bar{0}$), (1$\bar{2}$0), ($\bar{1}$20)	1.760	
(221)	1.718						
(10$\bar{1}$), (0$\bar{1}$1)	1.526		1.519	ms	($\bar{1}$11), ($\bar{1}\bar{1}$1)	1.525	1.510*
					(002)	1.483	
(210), (120)	1.427		1.427	w	(031), (0$\bar{3}$1)	1.435	1.434*
					(03$\bar{1}$)		
					(102)	1.433	
(102), (201), (021), (012)	1.381		1.381	w	(13$\bar{1}$), (1$\bar{3}$1), (211), (1$\bar{2}$2), (2$\bar{1}$1), (1$\bar{2}$2)	1.383 / 1.359	1.368*
(020), (200), (002)	1.268	1.241*			(202)	1.289	
(223)	1.235		1.236	ms	(200), (022), (02$\bar{2}$), (0$\bar{2}$2)	1.268	1.270*
(220)	1.221						
(202), (022)	1.137		1.151	w	(13$\bar{1}$), (1$\bar{3}$1)	1.147	1.144*
					(222), (2$\bar{2}$2),	1.141	
(213), (123)	1.098	1.090*	1.109	w	(220), ($\bar{2}$20), (2$\bar{2}$0)	1.125	
(11$\bar{3}$)	1.078						
(12$\bar{1}$), (21$\bar{1}$)	1.000	0.996*			(10$\bar{2}$)	1.086	
(10$\bar{2}$), ($\bar{2}$01)	0.993		1.008	f	(11$\bar{3}$), (1$\bar{1}$3)	1.076	1.080*
(0$\bar{1}$2), (02$\bar{1}$)					(231), (2$\bar{3}$1)	1.071	

s—strong, ms—medium strong, w—weak, f—faint. Weighted mean values indicated by *.

Results obtained from this equation are likewise tabulated in column 8. The calculated value of β is 67° 43′.

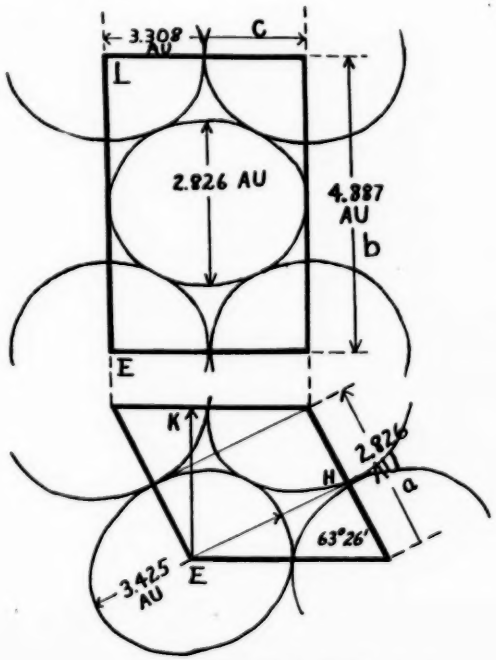

FIG. 2. The uranium cell.

So many of the reflections are now accounted for that it seems probable that $2K_{13}=2K_{23}$, hence $\beta=\gamma$. So the projection of g on the ef plane coincides with the bisector of δ. This situation produces the symmetry expected in the simple uranium cell, although the cell is triclinic.

Since $D_1=2.535$A from the x-ray data, a rearranged form of Eq. (7) for the simple triclinic uranium cell may be written:

$$2.535^2/D^2=h^2+k^2+l^2-0.9232hk-0.7576(h+k)l. \quad (12)$$

Columns 2 and 3 of Table II show the agreement obtained between the observed D values and those calculated by Eq. (12) for the planes shown in column 1.

The cell thus derived is shown in Fig. 1b. The volume of this simple cell (Eq. (8)) is 20.53A^3. The calculated density of uranium is 19.05, compared with the usually reported density of 18.68; a difference of 2.2 percent.

THE CRYSTALLOGRAPHIC CELL OF URANIUM

By a change in the choice of coordinate axes,

this simple cell may be converted into the monoclinic cell shown in Fig. 2. The crystallographic axes, a, b and c, are indicated. The face plane perpendiculars of this cell are EK, EH and EL, with the lengths 2.535, 2.966 and 4.887A, respectively. $\delta = 63° 26'$. The equation of this cell is:

$$2.966^2/D^2 = 1.368h^2 + 0.368k^2 + l^2 - 1.046hl. \quad (13)$$

The coordinates of the equivalent points of the cell are 000, $0\frac{1}{2}\frac{1}{2}$, which locates uranium in space group C_{2h}^3 of Wyckoff's tabulation.[9] According to the structure vector for this configuration, the planes producing reflection are those in which h, k and l satisfy the following conditions:

hkl all even, or all odd;

h even, kl odd; h odd, kl even.

Columns 3 and 6 of Table II show how the interplaner spacings of the permitted planes listed in column 5 agree with the observed spacings. The number of cooperating planes producing reflection is in satisfactory agreement with the observed intensities, if allowance is made for the natural decrease of x-ray intensity with increasing angle of reflection.

In this cell, $a = 2.829$A; $b = 4.887$A; $c = 3.308$A. The axial ratios are therefore 0.5791 : 1 : 0.6771.

As shown in Fig. 2, this structure corresponds to a close packing of prolate spheroids with minor axes $= a = 2.826$A, and major axis $= 2EH/3^{\frac{1}{2}} = 3.425$A. This appears to be the probable shape of the uranium atoms in the lattice.

[9] Wyckoff, *The Analytical Expression of the Results of the Theory of Space Groups*, Washington, 1922.

Magnetic Properties of the Iron-Nickel Alloys Under Hydrostatic Pressure

R. L. STEINBERGER, *Jefferson Laboratory, Harvard University*

(Received February 11, 1933)

A series of well annealed iron-nickel alloys in nominal steps of 10 percent Ni, including pure iron and pure nickel, has been examined for the effect of pressures, up to 12,500 kg/cm², on the magnetic flux density. The application of pressure to a well annealed specimen causes a relatively large change in flux, usually a decrease and an incomplete recovery on release of pressure. The recovery is reversible in the sense that the same curve of flux change is traced with each series of pressure applications, provided the measuring pressure does not exceed that first applied. The 30 percent Ni alloy is rendered nearly nonmagnetic by a pressure of 12,000 kg/cm². In the remaining metals pure iron exhibits the greatest and 90 percent Ni the smallest pressure change of flux. At constant field the different alloys exhibit various types of pressure changes of flux; linear, nonlinear and types exhibiting hysteresis.

METHOD AND EXPERIMENTAL PROCEDURE

THE high-pressure technique of Bridgman[1] has already been applied to the examination of the ferromagnetic properties of the pure metals, iron, nickel and cobalt, by Dr. Chi-Sun Yeh.[2] The method of the present investigation differs from that of Yeh principally in an improved annealing treatment. Small rings of rectangular section with an average radial thickness 0.2 cm, axial width 0.5 cm and average outside diameter 2.0 cm were cut from a series of vacuum fused iron nickel alloy plates very kindly prepared for this investigation by Dr. L. W. McKeehan at the Bell Telephone Laboratories. The alloys were prepared in nominal steps of 10 percent nickel from pure iron to pure nickel. The chemical analyses furnished by Dr. McKeehan with the alloys are given in Table I.

After machining, each ring was heated to 1100°C in a vacuum furnace, then slowly cooled to room temperature at the constant rate of 30°C per hour. Secondary windings of 500 to 800 turns of No. 40 silk covered wire were wound on the rings over an insulating layer of thin paper. The primary winding of 200 to 400 turns of No. 32 silk covered copper wire was placed on top of the secondary. The completed specimens were then placed, one at a time, in a steel cylinder in which a pressure of 12,500 kg/cm² could be developed.

The electrical measurements involve the familiar ring ballistic method and need not be described here. For some specimens the compensating method of Yeh[2] was used, wherein the flux linkage between the two windings on the specimen was balanced by an equal and opposite linkage between two external air core coils.

TABLE I. *Chemical analyses of iron-nickel alloys.*

Specimen numbers	Nickel (%)	Iron (%)	Manganese (%)
M.N. 1, M.A.S. M.A.S.R., M.A. 2	0.07	—	0.03
M.A. 27	10.09	89.0	0.32
M.A. 28	20.15	78.69	0.36
M.A. 29	30.02	68.85	0.38
M.A. 30	40.51	58.37	0.37
M.A. 31	50.04	49.08	0.34
M.A. 32	59.57	39.87	0.37
M.A. 33	69.27	30.03	0.42
M.A. 34	78.98	19.94	0.60
M.A. 35	89.22	10.25	0.40
M.A. 36	—	0.30	0.42

Two types of run were made, *constant pressure* and *constant field*. The first gave a *B–H* curve at a fixed pressure. In the second type the field was held fixed and the resulting change of *B* with pressure was measured. In general three constant pressure runs were made on each specimen at 30°C. A few were made at room temperature and a few at 75°C. The first run on each specimen, made at one atmosphere

[1] P. W. Bridgman, *The Technique of High Pressure Experimenting*, Amer. Acad. Arts and Sci. Proc. **49**, 627–643 (1914).

[2] Chi-Sun Yeh, *The Effect of Hydrostatic Pressure on the Magnetic Permeability of Iron, Cobalt and Nickel*, Am. Acad. Arts and Sci. Proc. **60**, 503–533 (1925).

immediately after annealing and called the primitive, serves to describe the original magnetic condition of the metal. The next run was made nominally at 12,000 kg/cm². The third was made at one atmosphere after release of pressure, and served to discover the permanent effect of pressure which is quite large in nearly all the specimens examined. All ballistic measurements were made at constant reversal (i.e., the measuring field was reversed a number of times until the ballistic deflection became constant before taking a reading) except in a few cases where the *first reversal* was recorded.

The effect of temperature and pressure in altering the flux and field measurements through changes in dimensions is small, not greater than 0.5 percent, but the effect was corrected for.

Discussion of Results

The tables of ballistic data and the detailed mechanical constants are too voluminous to include in this report. A thesis[3] presented at Harvard gives a full account of the work. The essential behavior of the alloys is clearly shown in the curve charts. The series of curves is not entirely complete. The 10 percent Ni alloy was omitted and the observations on the 70 percent Ni alloy were not completed because of lack of time. However, the essential behavior seems to be revealed clearly enough in spite of these omissions.

Constant pressure runs

In Figs. 1 to 8 are given the curves for the constant pressure runs. The general effect of a pressure of 12,000 kg/cm² is to cause a large initial decrease of flux density with only partial recovery on release of pressure. Pure iron, 60 percent and 90 percent nickel alloys, and pure

[3] R. L. Steinberger, *Magnetic Properties of the Iron Nickel Alloys under Hydrostatic Pressure*, Harvard Physics Thesis, February, 1932.

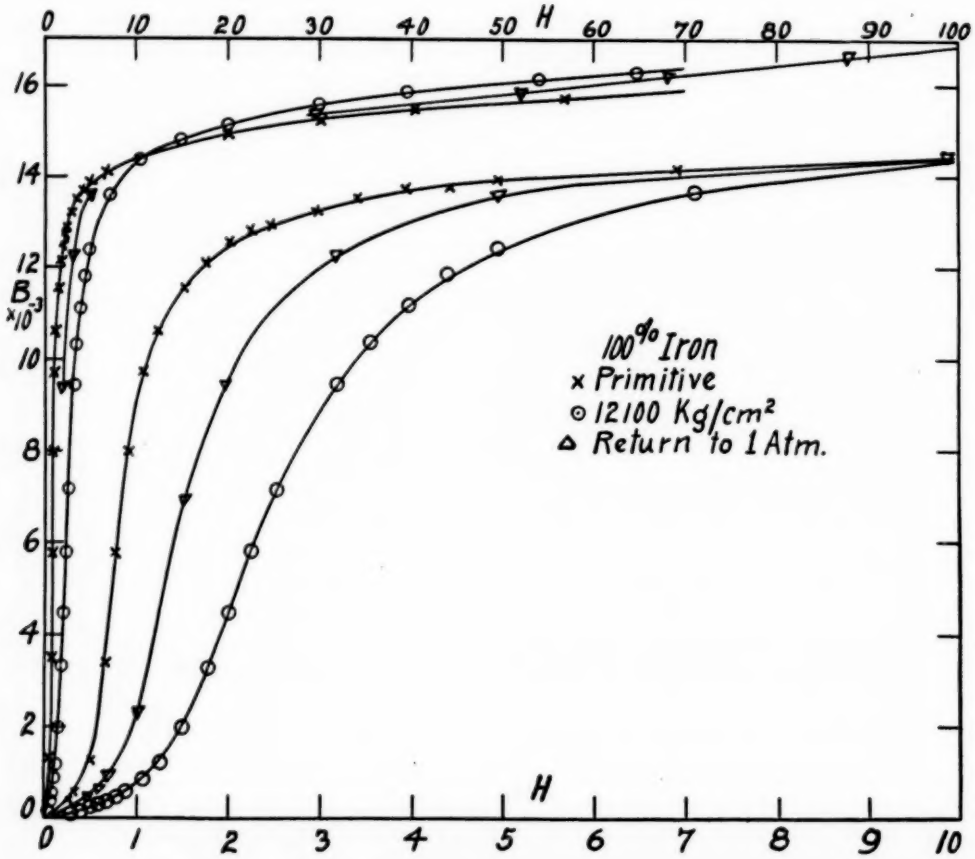

Fig. 1.

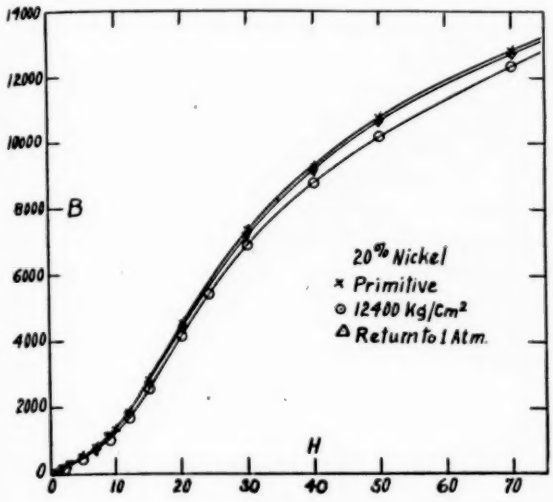

FIG. 2.

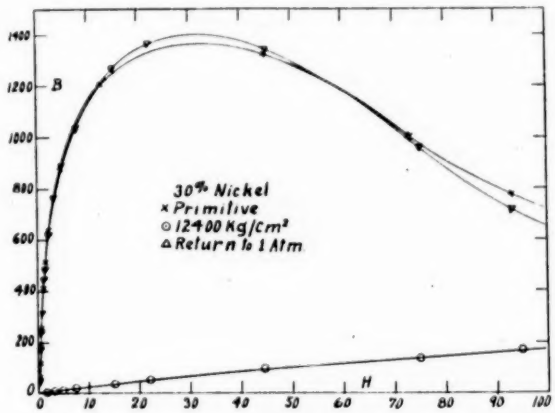

FIG. 3.

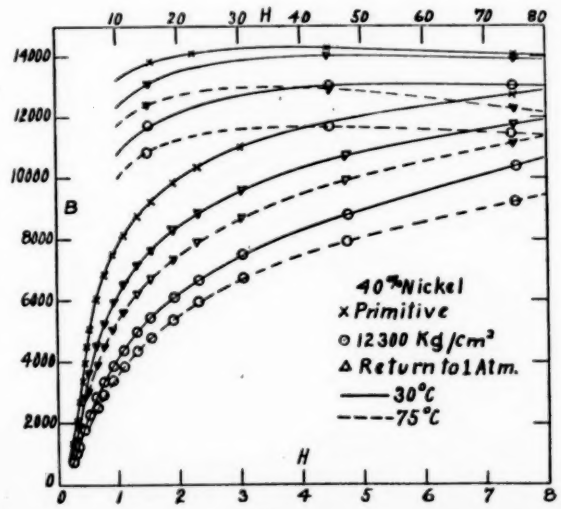

FIG. 4.

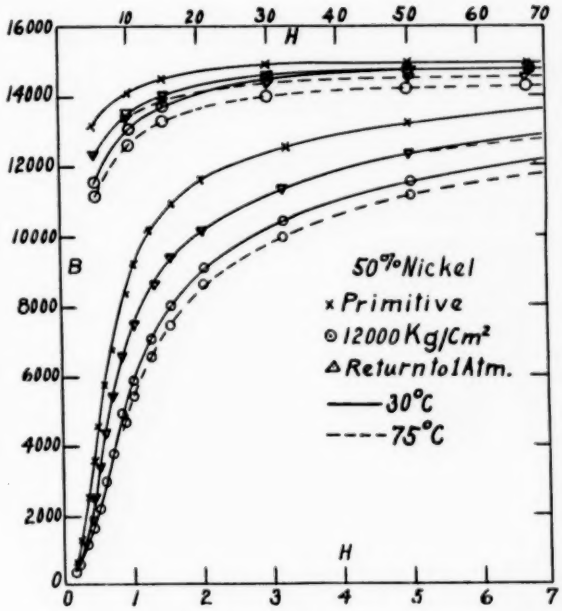

FIG. 5.

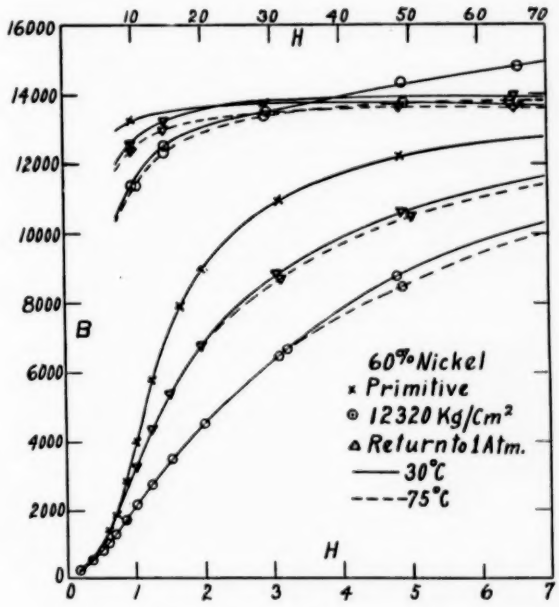

FIG. 6.

nickel, exhibit reversals in sign of the pressure effect—pure iron near $H=10$, 60 percent Ni between $H=20$ and $H=40$, 90 percent Ni near $H=1.5$ and pure nickel near $H=2$. In the 30 percent alloy the recovery is practically complete on release of pressure. This specimen is also unique because of the exceptionally large value

of the reversible change of flux with pressure which will be enlarged upon in the constant field run discussion.

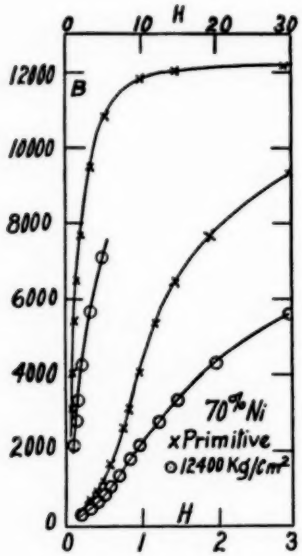

FIG. 7.

Temperature effects

The general effect of a rise in temperature in the range 30° to 75° is to cause a decrease in flux density. The droop in the constant pressure curves (Figs. 3 and 4) is due to the heating of the specimen by the magnetizing current in the restricted space of the pressure apparatus. In the 30 percent alloy the temperature coefficient is quite large, amounting to a decrease of 51 maxwells/cm² per degree at $H=7.5$, 30°C and at a pressure of one atmosphere.

Constant field runs

Figs. 9 to 18 list the constant field runs which reveal the percentage change in flux density at a fixed value of H as the pressure is raised and lowered. The constant field is not the same for all specimens. It was fixed at a figure near where the percentage change of flux is a maximum (see Fig. 20). The constant field curves exhibit a wide variety of forms. They indicate both positive and negative changes of flux with pressure. Most of the curves exhibit a decrease of flux. Fig. 18 for pure nickel exhibits a negative pressure coefficient because the fixed field ($H \equiv 14$) is well above the reversal point, which occurs near $H=2$. As Yeh has already found,[3] the pressure effect in pure iron is negative and linear near $H=2$. Two other specimens, 20 percent and 80 percent nickel, also exhibit linear changes. See Figs. 9, 10, 15.

The 30 percent Ni specimen exhibits nearly 100 percent decrease in flux density at 12,400 kg/cm² (Fig. 11). This alloy lies near the high nickel border of the region in the phase diagram of the iron nickel alloys[4] in which the mixed crystals of the solid solutions α_1 and α_2 can exist together. It also lies in the region where the Curie point chart[5] shows a sharp minimum. 30 percent Ni is about the concentration of the alloys which are nonmagnetic, with proper preparation, at room temperature. Fig. 3 shows that a pressure of 12,400 kg/cm² is sufficient to wipe out nearly all the flux density, making the metal a very weak ferromagnetic with a permeability about 1.7 which remains practically constant from $H=0$ to $H=100$. In Fig. 11 the percentage flux change with pressure as the field is held fixed at 7.48 is plotted. Unfortunately, much trouble was experienced with the pressure cylinder during the testing of this specimen, preventing a more complete investigation. The curves for the first two runs coincide quite well and probably indicate the true behavior of the metal. Both runs were terminated at 10,500 kg/cm² by accidental release of pressure. The first release was caused by a slow leak in the gauge plug packing—the second, by a violent explosion of the entire gauge plug. The pressure cylinder proved to be defective. Since the state of interval stress seems to be closely related to the magnetic quality of a ferromagnetic metal, an effect of the sudden fall of pressure was anticipated. The specimen was accordingly reexamined in another press and the third run was obtained which indicates an abrupt disappearance of ferromagnetism near 3200 kg/cm². If this curve represents a true state of the metal it must have been induced by the explosive release of pressure. In the neighborhood of 30 percent Ni, the specific volume at 0°C of the γ or nonmagnetic solid solution is less than that

[4] International Critical Tables, Vol. II, p. 451.

[5] *Invar and Related Nickel Steels*, Bur. Standards Circular, No. 58, p. 23, Fig. 12.

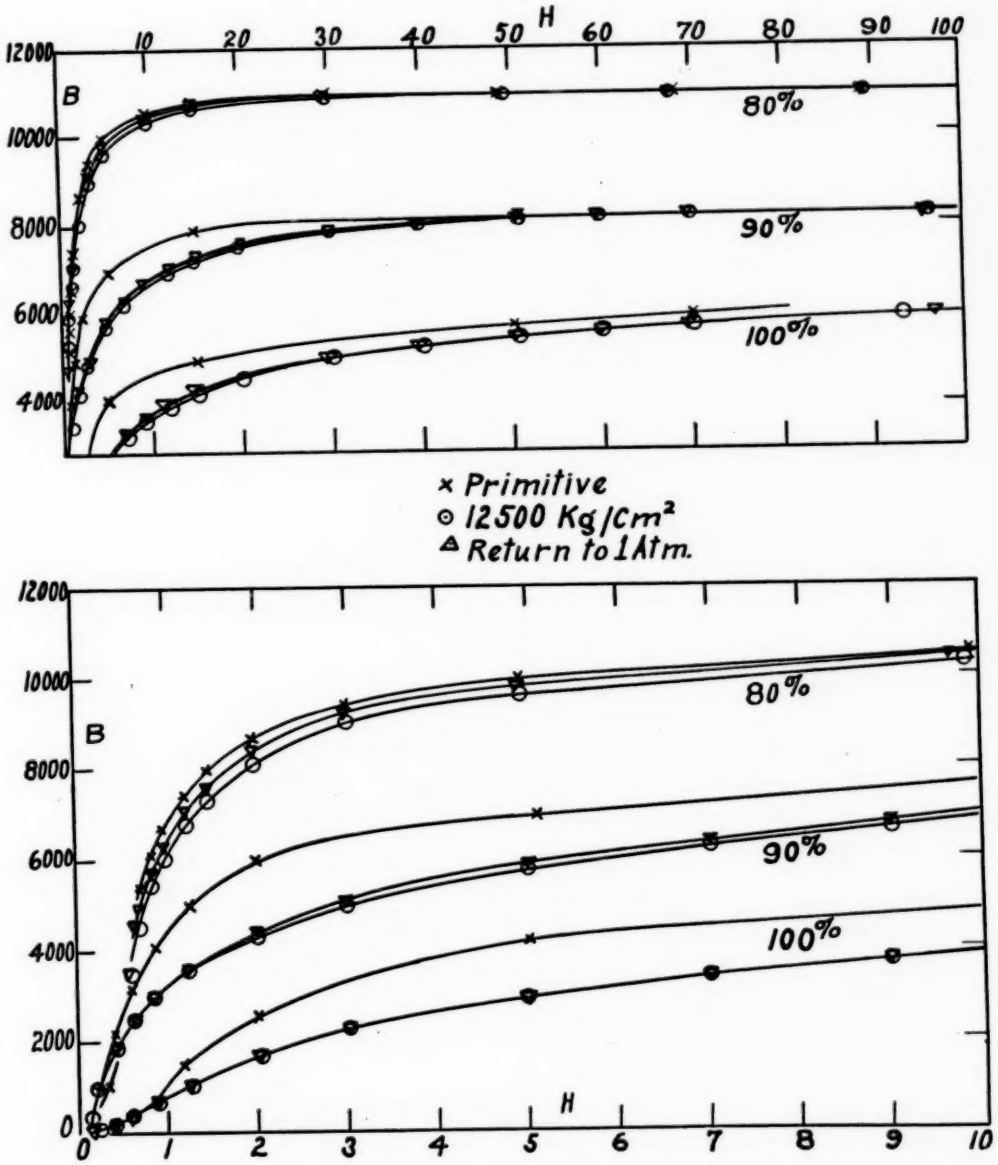

FIG. 8.

of the magnetic $(\alpha_1+\alpha_2)$ mixture.[6] In this specimen, therefore, pressure should favor the transformation to a nonmagnetic state.

At low fields 90 and 100 percent Ni reveal considerable hysteresis (Figs. 16, 17). That the flux does not return to its initial value on release of pressure in the case of 90 percent nickel is probably due to an inclusion of part of the initial irreversible flux decrease. At a higher field, $H=14$, the behavior of nickel reveals a curious hysteresis loop (Fig. 18). The mere reversal of sign of the pressure increment seems to cause a large additional flux change which is in the direction in which the flux had just been changing.

In Fig. 20 are plotted the reversible pressure changes of flux in percent per 1000 kg/cm² as determined by taking differences between the "12,000 kg" and *Return to one Atmosphere* constant pressure curves of Figs. 1 to 8. The top curve represents data from Yeh's paper.

[6] Reference 5, Fig. 41, p. 62.

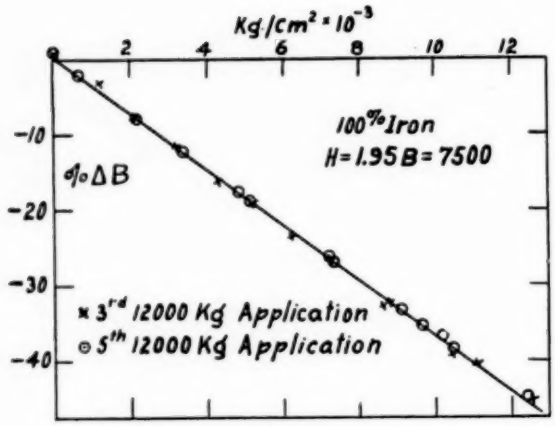

FIG. 9.

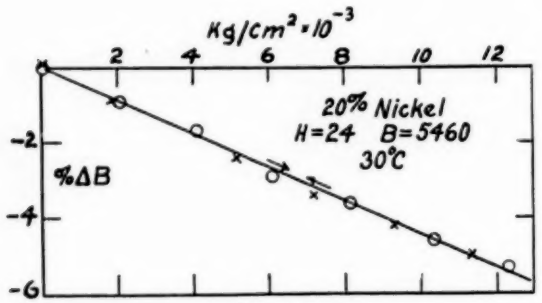

FIG. 10.

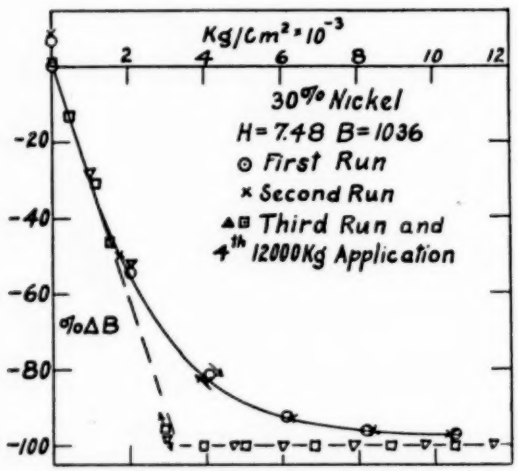

FIG. 11.

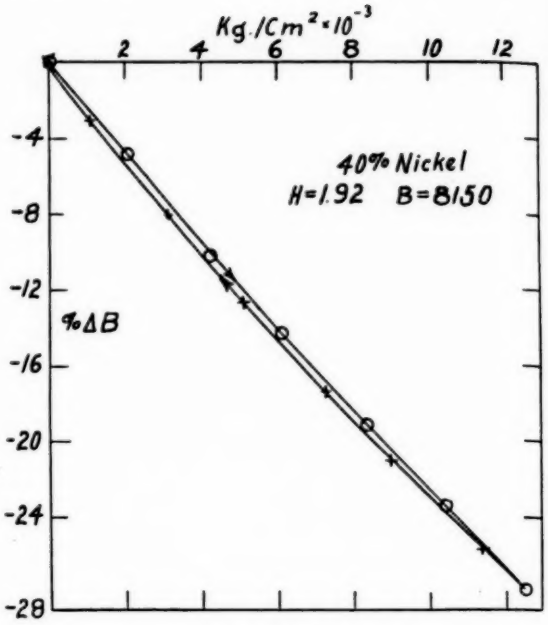

FIG. 12.

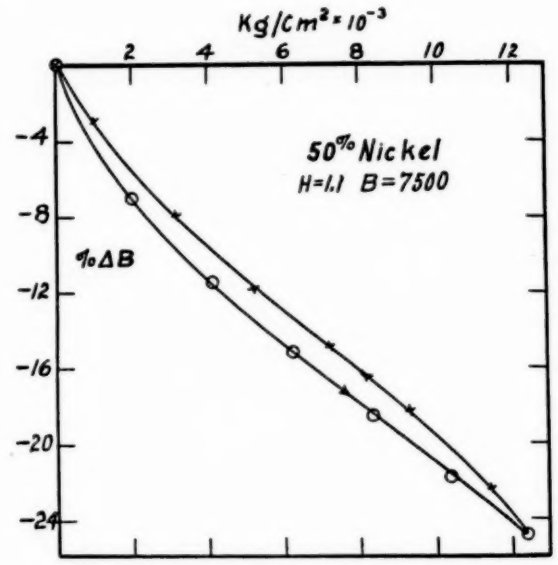

FIG. 13.

CONCLUSIONS

For all the alloys except 30 percent Ni, the following principal effects are to be noted.

(1) The first application of pressure causes a relatively large change, usually a decrease, in flux density, followed by incomplete recovery on release of pressure.

(2) The recovery is reversible in the sense that the flux changes give the same curve or hysteresis loop regardless of the number of times the pressure is applied, provided only that the measuring pressures never exceed the first or seasoning pressure.

(3) Reversible changes in flux are in many

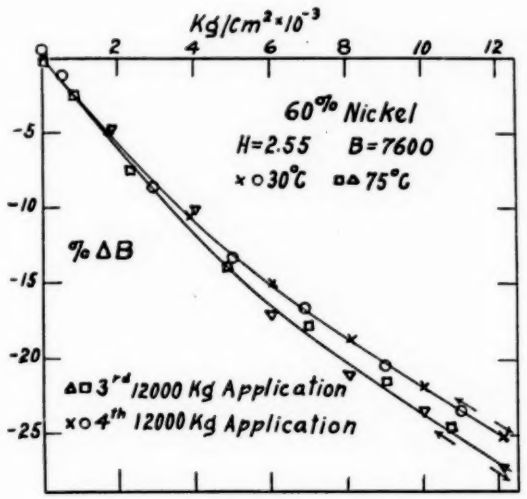

FIG. 14.

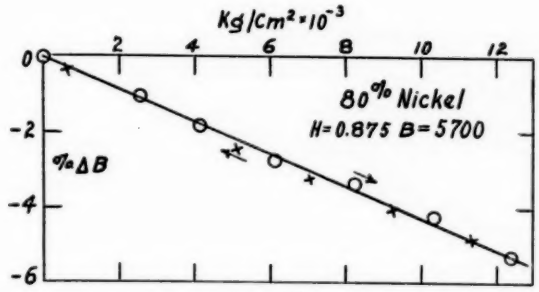

FIG. 15.

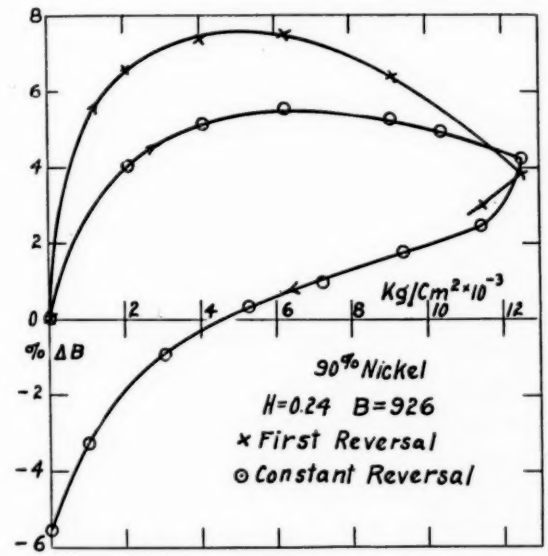

FIG. 16.

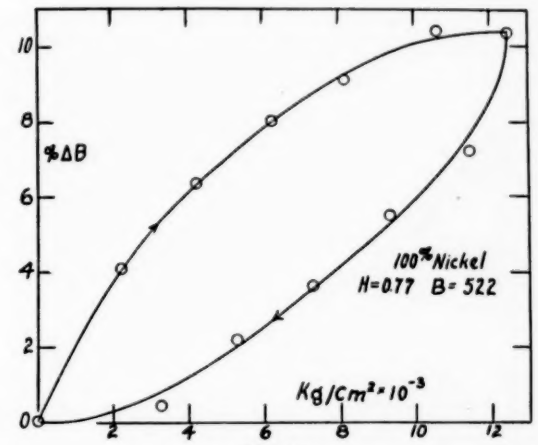

FIG. 17.

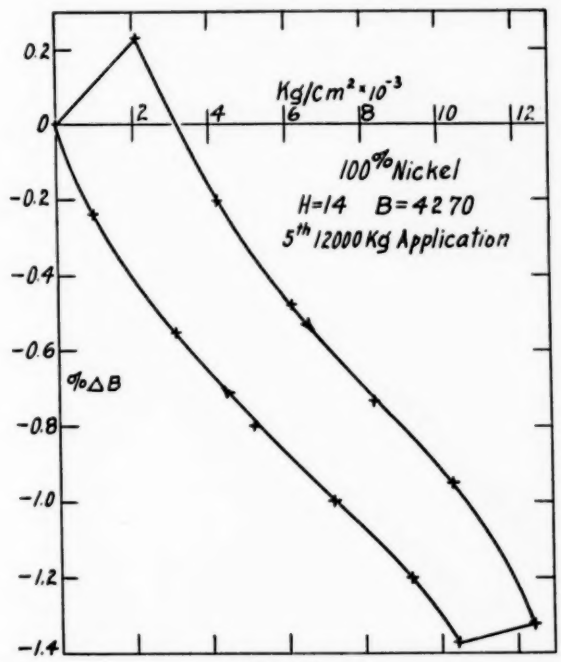

FIG. 18.

cases accompanied by hysteresis. Two values of flux density are found for one given value of pressure, depending upon the direction in which the pressure is changing, except at the terminal pressures where the two loop sides coincide.

(4) The rise of the *B–H* curve of a well annealed specimen is much sharper than that of one not annealed (Fig. 19). (This result, of course, is not new.)

(5) The effect of a good anneal in changing the flux density is opposite to and greater than the effect of a 12,000 kg/cm² application of pressure.

(6) The pressure effect may be positive or negative, depending upon the field strength applied.

(7) The field value at which the sign reversal in pressure effect occurs depends upon: (a) The temperature at which the measurements are made. (b) The extent of cold working to which the specimen had been subjected. (c) The kind of annealing process.

The results listed above suggest some kind of rearrangement of stress pattern within the crystal aggregate. It is well known[7] that the magnetic quality of a ferromagnetic metal is to a great extent dependent on the condition of internal strain existing within the metal at the time of testing and the work of Ruder[8] indicates that it is impossible to remove entirely all the strains in a specimen of steel by heating to temperatures less than the melting point. If such strains do exist in the metal, pressure may cause a shift in the strain pattern with accompanying changes in magnetic flux density similar to the effects observed by Fraichet[9] in a magnetic

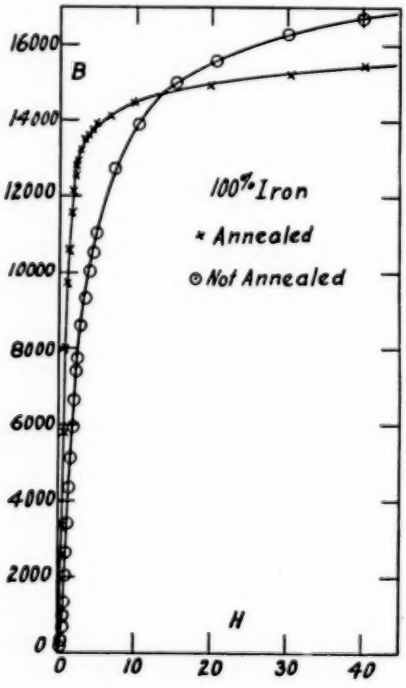

FIG. 19.

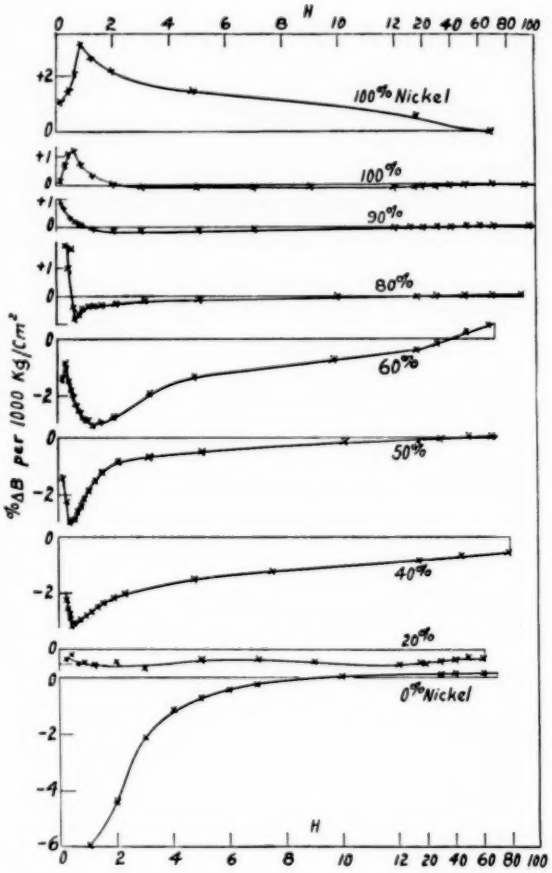

FIG. 20.

examination of iron and steel bars while subjected to simple tension. He found that with the first application of tension the flux density begins to decrease and falls rapidly and nearly linearly with increasing stress with a few superposed small discontinuities until a definite flux minimum is reached. Thereafter the flux rapidly recovers its original value. The recovery is however, not as smooth as the first decrease but is accompanied by many small jumps. The flux minimum is associated with an elastic limit (about half the usual engineering value) which Fraichet calls the "true elastic limit" above which internal readjustment begins. The flux recovery seems to be definitely associated with partial release of internal stress by this readjustment. Fridtjof Schmidt[10] has more recently

[7] T. D. Yensen, *Magnetic and Other Properties of Iron-Aluminum Alloys Melted in Vacuo*, Univ. Ill. Eng. Exp. Sta. Bull. No. 95, p. 30.

[8] W. E. Ruder, *Grain Growth in Silicon Steel*, Am. Inst. Min. & Engrs. Trans. **42**, 575 (1913).

[9] L. Fraichet, *Essai Magnetique des aciers a la traction limites elastique*, Revue de Metallurgie **20**, 549–559 (1923).

[10] Fridtjof Schmidt, *Investigation of the Induction of Iron in Tension Experiments*, Diss. Dresden, p. 475 (1931); Phys. Bericht. **12**, 1247 (1931).

carried out similar experiments on magnetic changes in steel while under tension.

Flux measurements such as recorded here are the net external effect of an internal magnetic field pattern of great complexity. The experiments of Bitter[11] on the external magnetic forces at the surface of single ferromagnetic crystals give information on the fine structure of the field and show the complexity of the magnetic field even in the ideally simple structure of single crystals. Because of the complexity of the problem a rational explanation of the curves submitted would be difficult to formulate.

The writer wishes to express his indebtedness to Dr. L. W. McKeehan for the preparation and chemical analyses of the alloys and to Professor P. W. Bridgman for full privileges in his laboratory.

[11] F. Bitter, *Experiments on the Nature of Ferromagnetism*, Phys. Rev. **41**, 507 (1932).

Direct Measurement of the Gravitational Effect of the Moon

KENNETH HARTLEY, *Hartley Gravity Balance Corporation, Houston, Texas*

(Received November 30, 1932)

The sensitivity of the gravity balance described in the March, 1932, number of *Physics* is such that a correction must be made for the effect of the attraction of the moon. This lunar effect has been measured by hourly readings over one complete cycle and agrees, within the observational error, with the effect calculated for the vertical component of the pull of the moon without any compensation for the centrifugal effect of the earth's motion around the center of gravity of the system. The effect has a period of 24.8 hours and not 12.4 hours as the tides, there is no trace of the twelve-hour period. Values of gravity plotted against time follow accurately a sine curve which shows a small time lag as compared with the theoretical curve. This does not seem to be accidental but has not been explained.

IN using the gravity balance described in the March, 1932, number of *Physics* for accurate measurements, it is necessary to make a correction for the effect of the moon. Our unit of measure is the millidyne, one-thousandth of a dyne per gram or 0.001 cm per sec.^{2} acceleration, and the effect of the moon when rising or setting changes at the rate of about 0.6 millidyne per hour, so that in checking back on a station five or six hours later than the original observation there might be a difference of three millidynes or more. I made a rough computation of this effect, using round numbers for distance and relative mass of the moon and the earth, for temporary use, and then decided that it would be worth while to make an actual measurement of it, keeping the balance in the same place for twenty-four hours or more.

Our location is rather close to the business section of Houston, and vibration from street traffic is bad, but a basement room under the rear end of the building proved much steadier than the ground floor so the measurement was attempted there. The first intention was merely to check the total difference from maximum to minimum, but readings in the basement room proved so satisfactory that it was decided to try hourly readings and see how closely the instrument could follow the gradual change.

When the ground is fairly steady it is possible to read the values of gravity quite definitely to one-fifth of a millidyne, but successive readings showed considerable irregularity. This was proved to be due to imperfect levelling. The instrument is intended for field use and so is mounted on a tripod and will not remain in adjustment very long but must be relevelled for each observation. It was found that a variation of one-fifth of a millidyne would be produced by a disturbance in level of not much more than one second, while we cannot level the present instrument closer than about five seconds. As the maximum variation between several successive readings did not exceed the amount attributable to imperfect levelling, it is believed that this is the only source of error, provided that the temperature is constant. In order to eliminate this error as far as possible the procedure adopted was to take five successive readings, relevelling each time, and use the mean of the five as the value for the time of the third reading. The results by this method were surprisingly close even when the deviation of individual readings was as much as 1.4 millidynes.

In the accompanying diagram the solid curve is a sine curve with a period of 24.8 hours and an amplitude equal to the measured variation in gravity. This was first drawn on transparent paper and fitted over the plotted points, as the best way to locate the exact time of maximum and minimum values, then redrawn on the diagram in that position. The points fit the curve so closely that it is impossible to shift it in either direction more than two or three minutes of time without noticeably departing from the logical position, yet the times of

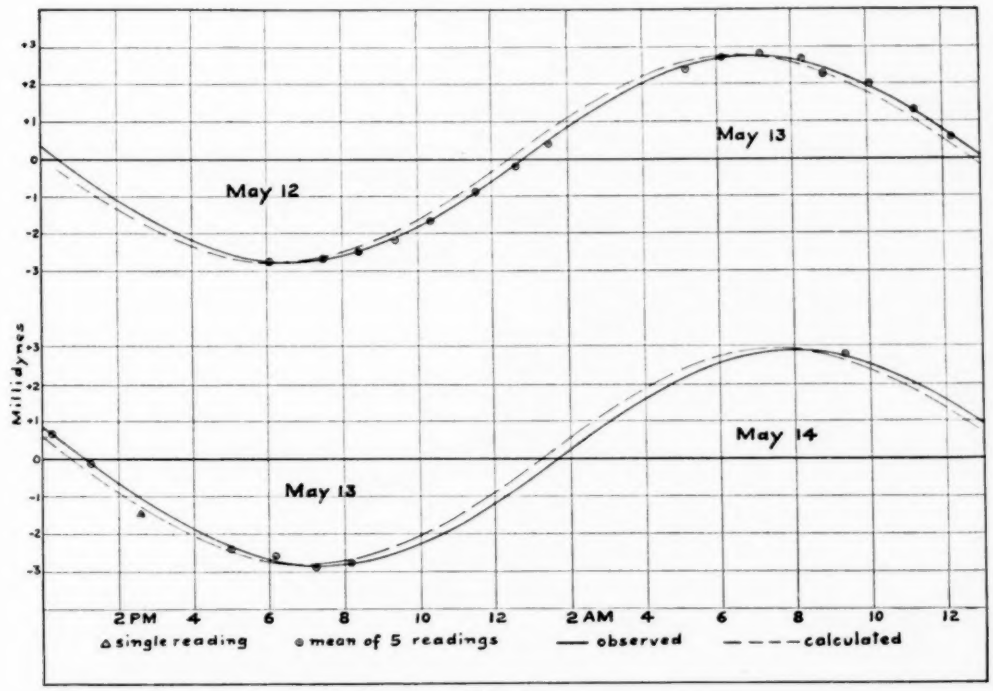

FIG. 1.

maximum and minimum do not agree with the times of transit of the moon across our meridian by about twenty-four minutes. The broken line in the diagram is a curve computed from astronomical data and based on the supposition that the instrument is measuring the total pull of the moon and not merely the differential effect which causes the tides. This differential effect would be only a fraction of the observed variation and would have a period of twelve hours instead of twenty-four. There is no suggestion of the twelve-hour period in this curve.

A preliminary set of readings was made on May 6, 1932, not as complete as the later set but enough to show the time of maximum and minimum quite closely, and the time lag was only about three minutes. This suggests that the larger lag on May 13 is due to the different position of the sun, but the computed effect of the sun is much too small to account for it.

It seems to me that a more extended series of observations, perhaps covering a full month or more, with a specially built instrument of greater precision, might give some very interesting results, but I am not in a position to do this so thought best to report these preliminary results without further delay.

The Gliding of a Snake

ARTHUR TABER JONES, *Smith College*

(Received February 15, 1933)

The snake is replaced by a model consisting of a number of spools separated by light pins and held together by rubber bands. The forces that act on one spool are considered. If the spool is in equilibrium between curved guides, and if the tensions in the rubber bands are altered in such a way that there is no change in the resultant longitudinal forces, but that the curvature of the given part of the model tends to increase, it is shown that there is a tendency to slip along the guides toward a region where the curvature is greater.

SEVERAL recent papers[1] deal with the gliding of snakes. A paper by Fokker, involving shearing stresses, is the only one in which the dynamical treatment is satisfactory. The following treatment does not involve shearing stresses, and it is simpler than Fokker's.

Mosauer's experimental work shows that when a snake is moving with the characteristic gliding motion which he calls "horizontal undulatory movement" the forces which the snake exerts on its surroundings are practically normal to its body. To simulate the path of a snake among grasses, twigs, or stones let a glass tube, large enough to admit the snake, be bent into a sinuous curve, and let the entire tube lie in a horizontal plane. If the snake-glass contact is really smooth, can the snake glide through the tube? If the snake's muscles are contracted in such a way that he naturally takes the shape of the tube he will be in equilibrium in it. If he changes his natural curvature to one which exists slightly farther along the tube, it seems likely that he will slip toward that part of the tube. The present note shows that this expectation is correct.

Let the snake be represented by a number of spools placed end to end. Let the spools be held together by rubber bands, and kept at a fixed distance apart by light pins that bear in conical depressions in plates on the ends of the spools. Fig. 1 shows the forces that act on one spool.

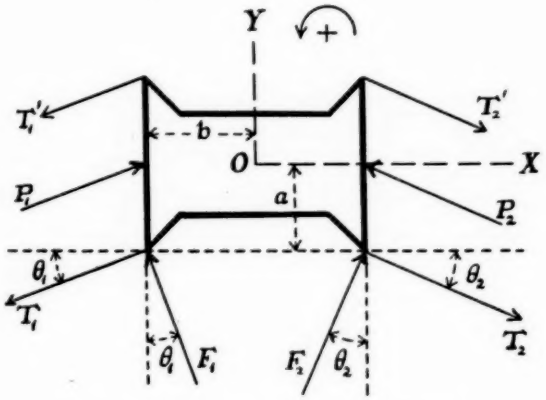

FIG. 1. The forces that act on one spool.

The T's are exerted by the rubber bands, the P's by the pins, and the F's by the glass tube. If the spools are almost in contact on the inner side of the curve the angles marked with the same symbols will be nearly equal.

Take the origin at O. Let the mass of the spool be m, and its radius of gyration about the Z axis be k. Write the three equations which state that the sum of the X components of the forces equals $m\ddot{x}$, the sum of the Y components equals $m\ddot{y}$, and the sum of the torques about the Z axis equals $mk^2\dot{\omega}$—the positive sign for the torques being that indicated in the figure. Let (1) stand for these three equations when the spool is in equilibrium. In this case $\ddot{x}=\ddot{y}=\dot{\omega}=0$.

Now let the tensions in the rubber bands be changed in such a way that the resultant of the forces which the adjacent spools exert on the given spool is not changed, but that the torques which they exert on it are changed. To accomplish this let T_1 and T_2 become respectively

[1] A. D. Fokker, Physica **7**, 65, 120 (1927). H. J. van Leeuwen, Physica **7**, 119, 121 (1927). Eduard Wiedemann, Zoologische Jahrbücher, Abt. f. allgem. Zool. u. Physiol. d. Tiere **50**, 557 (1932). Walter Mosauer, ibid. **52**, 191 (1932); Science **76**, 583 (1932).

$T_1+\epsilon$ and $T_2+\epsilon$, T_1' and T_2' become $T_1'-\epsilon$, and $T_2'-\epsilon$, P_1 and P_2 be unchanged, and F_1 and F_2 become $F_1+\epsilon_1'$ and $F_2+\epsilon_2'$. Let (2) stand for the three equations that correspond to (1) under the new conditions. If the spool is no longer in equilibrium it will start to move, and at this instant we shall have $\ddot{x}\neq 0$, $\ddot{y}=0$, $\dot{\omega}\neq 0$. Subtract the three Eqs. (1) from the three Eqs. (2), and from the three resulting equations eliminate ϵ_1' and ϵ_2'. We obtain

$$m\ddot{x}\{a+(2b\cos\theta_1\cos\vartheta_2)/(\sin(\theta_1+\theta_2))\} = mk^2\dot{\omega}+2\epsilon a(\cos\theta_1-\cos\theta_2). \quad (3)$$

This equation involves both $\ddot{x}$ and $\dot{\omega}$. To obtain another relation between these quantities consider the rotation of the given spool when it has moved to the right far enough to take the place of the next spool. If c stands for the length of a pin, and φ for the angle through which the spool turns, we have approximately

$$x=2b+c, \quad \varphi=-2\theta_2, \quad x=\tfrac{1}{2}\ddot{x}t^2, \quad \text{and} \quad \varphi=\tfrac{1}{2}\dot{\omega}t^2.$$

From these four equations eliminate x, φ, and t, and we see that

$$\dot{\omega}=-[2\theta_2/(2b+c)]\ddot{x}. \quad (4)$$

From (3) and (4) eliminate $\dot{\omega}$, and we get

$$m\ddot{x}\left\{a+\frac{2b\cos\theta_1\cos\theta_2}{\sin(\theta_1+\theta_2)}+\frac{2k^2\theta_2}{2b+c}\right\} = 2\epsilon a(\cos\theta_1-\cos\theta_2). \quad (5)$$

If the part of the tube in the neighborhood of the given spool either is straight or forms an arc of a circle, we have $\theta_2=\theta_1$, and therefore from (5) $\ddot{x}=0$. So if the whole tube is straight or circular, and if it is really smooth, the snake will be unable to work its way through it. The snake-glass contact is of course not really smooth. In fact, it is stated[2] that a snake can climb a vertical glass wall. But let us continue with the assumption that the contact is smooth.

If $\theta_2>\theta_1$, (5) shows that $\ddot{x}$ has the same sign as ϵ. That is, if the muscular action of the snake tends to produce a greater curvature in any short length of its body, it also produces a tendency for that part to slip toward a neighboring region of the tube where the curvature is greater, and *vice versa*. We see also that $\ddot{x}$ is proportional to $(\cos\theta_1-\cos\theta_2)$. If the curvature of the tube is the same at both ends of the spool we must have $\theta_2=\theta_1$. The more rapidly the curvature changes as we pass along the tube the greater is the difference between θ_2 and θ_1. So the force that urges the snake along the tube is greatest where the curvature is changing most rapidly. This result agrees with that obtained theoretically, but quite differently, by Fokker, and it is also in accord with the result obtained experimentally by Mosauer.

---

[2] H. F. Hutchinson, Nature **20**, 528 (1879).